

1      **A probabilistic framework for the cover effect in bedrock erosion**

2

3

4      Jens M. Turowski

5      *Helmholtzzentrum Potsdam, German Research Centre for Geosciences GFZ, Telegrafenberg, 14473*

6      *Potsdam, Germany, turowski@gfz-potsdam.de*

7      Rebecca Hodge

8      *Department of Geography, Durham University, Durham, DH1 3LE, United Kingdom,*

9      *rebecca.hodge@durham.ac.uk*

10

11

12      **Abstract**

13      The cover effect in fluvial bedrock erosion is a major control on bedrock channel morphology and long-  
14      term channel dynamics. Here, we suggest a probabilistic framework for the description of the cover  
15      effect that can be applied to field, laboratory and modelling data and thus allows the comparison of  
16      results from different sources. The framework describes the formation of sediment cover as a function  
17      of the probability of sediment being deposited on already alluviated areas of the bed. We define  
18      benchmark cases and suggest physical interpretations of deviations from these benchmarks.  
19      Furthermore, we develop a reach-scale model for sediment transfer in a bedrock channel and use it to  
20      clarify the relations between the sediment mass residing on the bed, the exposed bedrock fraction and  
21      the transport stage. We derive system time scales and investigate cover response to cyclic  
22      perturbations. The model predicts that bedrock channels achieve grade in steady state by adjusting  
23      bed cover. Thus, bedrock channels have at least two characteristic time scales of response. Over short  
24      time scales, the degree of bed cover is adjusted such that they can just transport the supplied sediment  
25      load, while over long time scales, channel morphology evolves such that the bedrock incision rate  
26      matches the tectonic uplift or base level lowering rate.

27

28      **1. Introduction**

29

30      Bedrock channels are shaped by erosion caused by countless impacts of the sediment particles they  
31      carry along their bed (Beer and Turowski, 2015; Cook et al., 2013; Sklar and Dietrich, 2004). There are  
32      feedbacks between the evolving channel morphology, the bedload transport, and the hydraulics  
33      (e.g., Finnegan et al., 2007; Johnson and Whipple, 2007; Wohl and Ikeda, 1997). Impacting bedload  
34      particles driven forward by the fluid forces erode and therefore shape the bedrock bed. In turn, the  
35      morphology of the channel determines the pathways of both sediment and water, and sets the stage  
36      for the entrainment and deposition of the sediment (Hodge and Hoey, 2016). Sediment particles play  
37      a key role in this erosion process; they provide the tools for erosion and also determine where  
38      bedrock is exposed such that it can be worn away by impacting particles (Gilbert, 1877; Sklar and  
39      Dietrich, 2004).

40

41      The importance of the cover effect - that a stationary layer of gravel can shield the bedrock from  
42      bedload impacts – has by now been firmly established in a number of field and laboratory studies  
43      (e.g., Chatanantavet and Parker, 2008; Finnegan et al., 2007; Hobley et al., 2011; Johnson and  
44      Whipple, 2007; Turowski and Rickenmann, 2009; Turowski et al., 2008; Yanites et al., 2011).

45      Sediment cover is generally modelled with generic relationships that predict the decrease of the  
46      fraction of exposed bedrock area  $A^*$  with the increase of the relative sediment supply  $Q_s^*$ , usually  
47      defined as the ratio of sediment supply to transport capacity. Based on laboratory experiments and  
48      simple modeling, Turowski and Bloem (2016) argued that the focus on covered area is generally

49 justified on the reach scale and that erosion of bedrock under a thin sediment cover can be  
50 neglected. However, the behavior of sediment cover under flood conditions is currently unknown  
51 and the assumption that the cover distribution at low flow is representative for that at high flow may  
52 not be justified (cf. Beer et al., 2016; Turowski et al., 2008).

53  
54 The most commonly used function to describe the cover effect is the linear decline (Sklar and  
55 Dietrich, 1998), which is the simplest function connecting the steady state end members of an empty  
56 bed when relative sediment supply  $Q_s^* = 0$  and full cover when  $Q_s^* = 1$ :

57

$$58 A^* = \begin{cases} 1 - Q_s^* & \text{for } Q_s^* < 1 \\ 0 & \text{otherwise} \end{cases}$$

59 (eq. 1)

60 In contrast, the exponential cover function arises under the assumption that particle deposition is  
61 equally likely for each part of the bed, whether it is covered or not (Turowski et al., 2007).

62

$$63 A^* = \begin{cases} \exp(-Q_s^*) & \text{for } Q_s^* < 1 \\ 0 & \text{otherwise} \end{cases}$$

64 (eq. 2)

65 Here,  $\exp$  denotes the natural exponential function.

66  
67 Hodge and Hoey (2012) obtained both the linear and the exponential functions using a cellular  
68 automaton (CA) model that modulated grain entrainment probabilities by the number of  
69 neighbouring grains. However, consistent with laboratory flume data, the same model also produced  
70 other behaviours under different parameterisations. One alternative behavior is runaway alluviation,  
71 which was attributed by Chatanantavet and Parker (2008) to the differing roughness of bedrock and  
72 alluvial patches. Due to a decrease in flow velocity, an increase in surface roughness and differing  
73 grain geometry, the likelihood of deposition is higher over bed sections covered by alluvium  
74 compared to smooth, bare bedrock sections (Hodge et al., 2011). This can lead to rapid alluviation of  
75 the entire bed once a minimum fraction has been covered. The relationship between sediment flux  
76 and cover is also affected by the bedrock morphology; flume experiments have demonstrated that  
77 on a non-planar bed the location of sediment cover is driven by bed topography and hydraulics (e.g.,  
78 Finnegan et al., 2007; Inoue et al., 2014). Johnson and Whipple (2007) found that stable patches of  
79 alluvium tended to form in topographic lows such as pot holes and at the bottom of slot canyons,  
80 whereas Hodge and Hoey (2016) found that local flow velocity also controls sediment cover location.

81  
82 The relationship between roughness, bed cover and incision was explored in a number of recent  
83 numerical modeling studies. Nelson and Seminara (2011, 2012) were one of the first to model the  
84 impact that the differing roughness of bedrock and alluvial areas has on sediment patch stability.  
85 Zhang et al. (2014) formulated a macro-roughness cover model, in which sediment cover is related to  
86 the ratio of sediment thickness to bedrock macro-roughness. Aubert et al. (2016) directly simulated  
87 the dynamics of particles in a turbulent flow and obtained both linear and exponential cover  
88 functions. Johnson (2014) linked erosion and cover to bed roughness in a reach-scale model. Using a  
89 model formulation similar to that of Nelson and Seminara (2011), Inoue et al. (2016) reproduced bar  
90 formation and sediment dynamics in bedrock channels. All of these studies used slightly different  
91 approaches and mathematical formulations to describe alluvial cover, making a direct comparison  
92 difficult.

93  
94 Over time scales including multiple floods, the variability in sediment supply is also important (e.g.,  
95 Turowski et al., 2013). Lague (2010) used a model formulation in which cover was written as a

96 function of the average sediment depth to upscale daily incision processes to long time scales. He  
97 found that over the long term, cover dynamics are largely independent of the precise formulation at  
98 the process scale and are rather controlled by the magnitude-frequency distribution of discharge and  
99 sediment supply. Using the CA model of Hodge and Hoey (2012), Hodge (in press) found that, when  
100 sediment supply was very variable, sediment cover was primarily determined by the recent history of  
101 sediment supply, rather than the relationships identified under constant sediment fluxes.

102  
103 So far, it has been somewhat difficult to compare and discuss the different cover functions obtained  
104 from theoretical considerations, numerical models, and experiments, since a unifying framework and  
105 clear benchmark cases have been missing. Here, we propose such a framework, and develop type  
106 cases linked to physical considerations of the flow hydraulics and sediment erosion and deposition.  
107 We show how this framework can be applied to data from a published model (Hodge and Hoey,  
108 2012). Furthermore, we develop a reach-scale erosion-deposition model that allows the dynamic  
109 modeling of cover and prediction of steady states. Thus, we clarify the relationship between cover,  
110 deposited mass and relative sediment supply. As part of this model framework we investigate the  
111 response time of a channel to a change in sediment input, which we illustrate using data from a  
112 natural channel.

## 114 2. A probabilistic framework

### 115 2.1. Development

116 Here we build on the arguments put forward by Turowski et al. (2007) and Turowski (2009). Consider  
117 a bedrock bed on which sediment particles are distributed. We can view the deposition of each  
118 particle as a random process, and each area element on the bed surface can be assigned a probability  
119 for the deposition of a particle. When assuming that a given number of particles are distributed on  
120 the bed, the mean behavior of the exposed area  $A^*$  can be calculated from the following equation:

$$122 dA^* = -P(A^*, M_s^*, \dots) dM_s^*$$

123 (eq. 3)

124  $P$  is the probability that a given particle is deposited on the exposed part of the bed, which here is a  
125 function of the fraction of exposed area ( $A^*$ ) and a dimensionless mass of particles on the bed per  
126 area ( $M_s^*$ , explained below), but which can be expected to also be a function of the relative sediment  
127 supply, the bed topography and roughness, the particle size, the local hydraulics or other control  
128 variables.  $M_s^*$  is a dimensionless mass equal to the total mass of the particles residing on the bed per  
129 area, which is suitably normalized. A suitable mass for normalization is the minimum mass required  
130 to cover a unit area,  $M_0$ , as will become clear later. The minus sign is introduced because the fraction  
131 of the exposed area reduces as  $M_s^*$  increases. Similar to eq. (3), the equation for the fraction of  
132 covered area  $A_c^* = 1 - A^*$  can be written as:

$$134 dA_c^* = P(A^*, M_s^*, \dots) dM_s^*$$

135 (eq. 4)

136 As most previous relationships are expressed in terms of relative sediment supply  $Q_s^*$ , the relation of  
137  $M_s^*$  to  $Q_s^*$  will be discussed later.

138  
139 We can make some general statements about  $P$ . First,  $P$  is defined for the range  $0 \leq A^* \leq 1$  and  
140 undefined elsewhere. Second,  $P$  takes values between zero and one for  $0 \leq A^* \leq 1$ . Third,  $P(A^*=0) = 0$   
141 and  $P(A^*=1) = 1$ . Note that  $P$  is not a distribution function and therefore does not need to integrate  
142 to one. Neither does it have to be continuous and differentiable everywhere.

144 For purpose of illustration, we will next discuss two simple forms of the probability function  $P$  that  
 145 lead to the linear and exponential forms of the cover effect, respectively. First, consider the case that  
 146 all particles are always deposited on exposed bedrock. In this case, formally, to keep with the  
 147 conditions stated above, we define  $P = 1$  for  $0 < A^* \leq 1$  and  $P = 0$  for  $A^* = 0$ . Thus, we can write  
 148

$$149 \quad dA^* = -dM_s^* \quad \text{for } 0 < A^* \leq 1 \\ dA^* = 0 \quad \text{for } A^* = 0$$

150 (eq. 5)

151 Integrating, we obtain:

$$152 \quad A^* = -M_s^* + C$$

153 (eq. 6)

154 where the constant of integration  $C$  is found to equal one by using the condition  $A^*(M_s^* = 0) = 1$ . Thus,  
 155 we obtain the linear cover function of eq. (1). Note that the linear cover function gives a theoretical  
 156 lower bound for the amount of cover: it arises when all available sediment always falls on uncovered  
 157 ground, and thus no additional sediment is available that could facilitate quicker alluviation. In  
 158 essence, this is a mass conservation argument. Now it is obvious why  $M_0$  is a convenient way to  
 159 normalize: in plots of  $A^*$  against  $M_s^*$ , we obtain a triangular region bounded by the points  $[0,1]$ ,  $[0,0]$   
 160 and  $[1,0]$  in which the cover function cannot exist (Fig. 1).

161

162 Similarly to above, if we set  $P$  to a constant value smaller than one for  $0 < A^* \leq 1$ , we obtain  
 163

$$164 \quad A^* = 1 - kM_s^*$$

165 (eq. 7)

166 It is clear that the assumption of  $P = k$  is physically unrealistic, because it implies that the probability  
 167 of deposition on exposed ground is independent of the amount of uncovered bedrock. Especially  
 168 when  $A^*$  is close to zero, it seems unlikely that, say, always 90% of the sediment falls on uncovered  
 169 ground. A more realistic assumption is that the probability of deposition on uncovered ground is  
 170 independent of location and other possible controls, but is equal to the fraction of exposed area, i.e.,  
 171  $P = A^*$ . In a probabilistic sense, this is also the simplest plausible assumption one can make. Then  
 172

$$173 \quad dA^* = -A^* dM_s^*$$

174 (eq. 8)

175 giving upon integration

$$176 \quad A^* = e^{-M_s^*}$$

177 (eq. 9)

178 The argument used here to obtain the exponential cover effect in eq. (9) essentially corresponds to  
 179 the one given by Turowski et al. (2007). Since this case presents the simplest plausible assumption,  
 180 we will use it as a benchmark case, to which we will compare other possible functional forms of  $P$ .  
 181

182 In principle, the probability function  $P$  can be varied to account for various processes that make  
 183 deposition more likely either on already covered ground by decreasing  $P$  for the appropriate range of  
 184  $A^*$  from the benchmark case  $P = A^*$ , or on uncovered ground by increasing  $P$  from the benchmark  
 185 case  $P = A^*$ . As has been identified previously (Chatanantavet and Parker, 2008; Hodge and Hoey  
 186 2012), roughness feedbacks to the flow can cause either case depending on whether subsequent  
 187 deposition is adjacent to or on top of existing sediment patches. In the former case, particles residing  
 188 on an otherwise bare bedrock bed act as obstacles for moving particles, and create a low-velocity  
 189 wake zone in the downstream direction. In addition, particles residing on other single particles are  
 190 unstable and stacks of particles are unlikely. Hence, newly arriving particles tend to deposit either  
 191 upstream or downstream of stationary particles and the probability is generally higher for deposition

192 on uncovered ground than in the benchmark case. In the latter case, larger patches of stationary  
193 particles increase the surface roughness of the bed, thus decreasing the local flow velocity and  
194 stresses, making deposition on the patch more likely. In this way, the probability of deposition on  
195 already covered bed is increased in comparison to the benchmark case.

196  
197 A simple functional form that can be used to take into account either one of these two effects is a  
198 power law dependence of  $P$  on  $A^*$ , taking the form  $P = A^{*\alpha}$  (Fig. 1A). Then, the cover function  
199 becomes (Fig. 1B):

200  
201 
$$A^* = (1 - (1 - \alpha)M_s^*)^{\frac{1}{1-\alpha}}$$

202 (eq. 10)

203 Here, the probability of deposition on uncovered ground is increased in comparison to the  
204 benchmark exponential case if  $0 < \alpha < 1$ , and decreased if  $\alpha > 1$ .

205  
206 A convenient and flexible way to parameterize  $P(A^*)$  in general is the cumulative version of the Beta  
207 distribution, given by:

208 
$$P(A^*) = B(A^*; a, b)$$

209 (eq. 11)

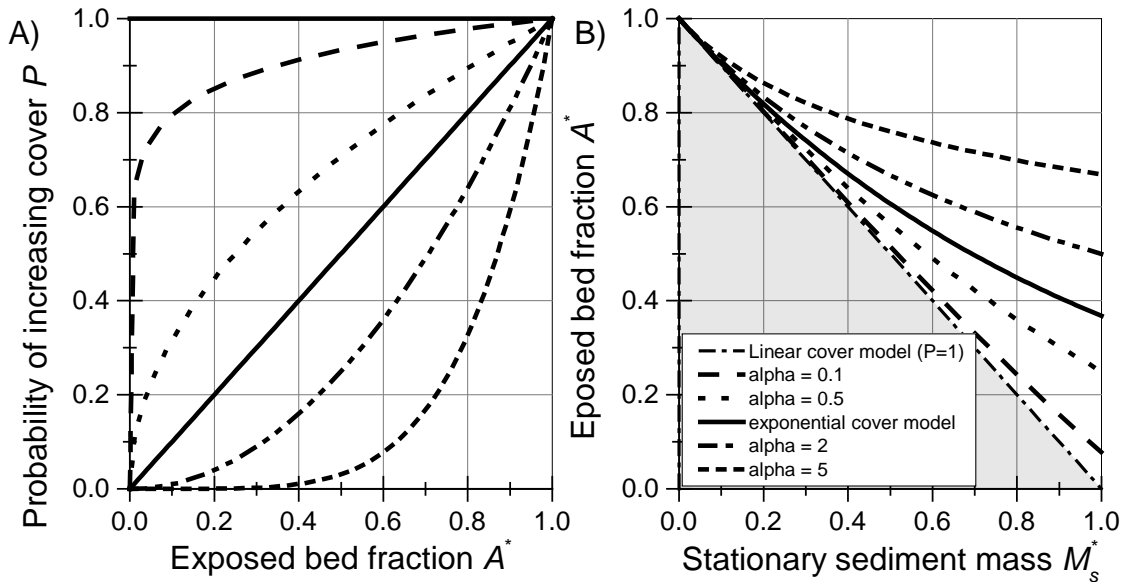
210 Here,  $B(A^*; a, b)$  is the regularized incomplete Beta function with two shape parameters  $a$  and  $b$ ,  
211 which are both real positive numbers, defined by:

212 
$$B(A^*; a, b) = \frac{\int_0^{A^*} y^{a-1} (1-y)^{b-1} dy}{\int_0^1 y^{a-1} (1-y)^{b-1} dy}$$

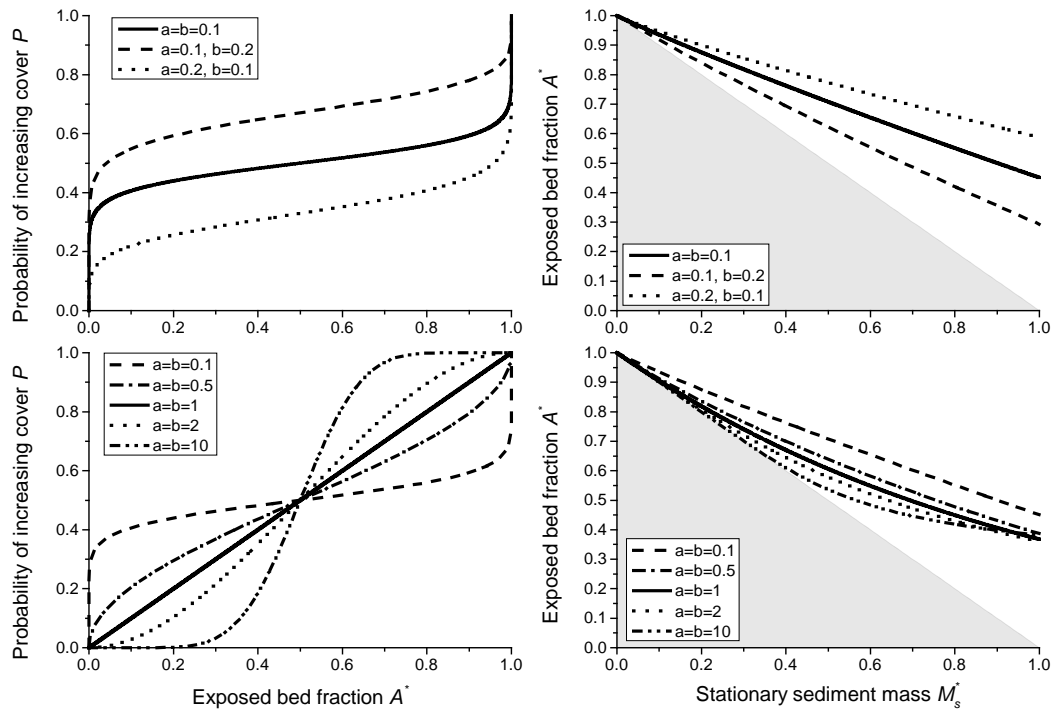
213 (eq. 12)

214 Here,  $y$  is a dummy variable. With suitable choices for  $a$  and  $b$ , cover functions resembling the  
215 exponential ( $a=b=1$ ), the linear form ( $a=0, b>0$ ), and the power law form ( $a>>b$  or  $a<<b$ ) can be  
216 retrieved. Wavy functions are also a possibility (Fig. 2), thus both of the roughness effects described  
217 above can be modelled in a single scenario. Unfortunately, the integral necessary to obtain  $A^*(M_s^*)$   
218 does not give a closed-form analytical solution and needs to be computed numerically.

219  
220 In principle, a suitable function  $P$  could also be defined to account for the influence of bed  
221 topography on sediment deposition. Such a function is likely dependent on the details of the  
222 particular bed, hydraulics and sediment flow paths in a complex way and needs to be mapped out  
223 experimentally.



225  
226 Fig. 1: A) Various examples for the probability function  $P$  as a function of bedrock exposure  $A^*$ . B)  
227 Corresponding analytical solutions for the cover function between  $A^*$  and dimensionless sediment  
228 mass  $M_s^*$  using eq. (7), (9) and (10). Grey shading depicts the area where the cover function cannot  
229 run due to conservation of mass.  
230



231  
232 Fig. 2: Examples for the use of the regularized incomplete Beta function (eq. 12) to parameterize  $P$ ,  
233 using various values for the shape parameters  $a$  and  $b$ . The choice  $a = b = 1$  gives a dependence that  
234 is equivalent to the exponential cover function. Grey shading depicts the area where the cover  
235 function cannot run due to conservation of mass.  
236

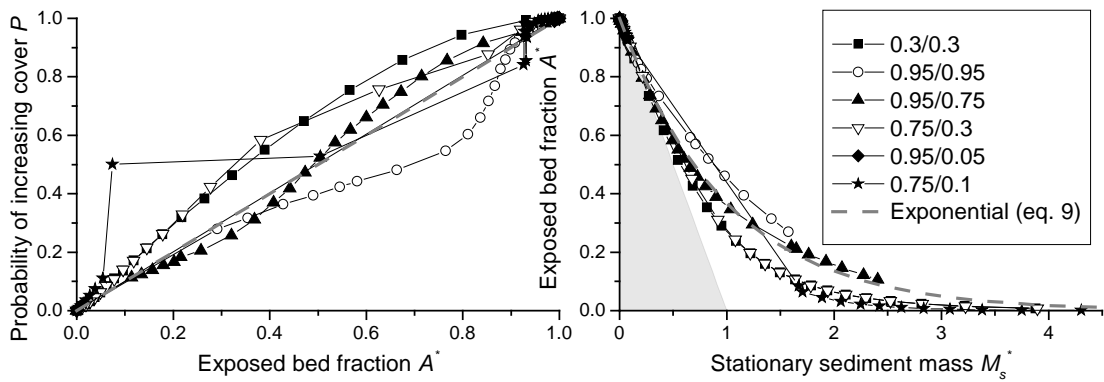
237 **2.2 Example of application using model data**

238  
239 To illustrate how the framework can be used, we apply it to data obtained from the CA model  
240 developed by Hodge and Hoey (2012). The CA model reproduces the transport of individual sediment  
241 grains over a smooth bedrock surface. In each time step, the probability of a grain being entrained is  
242 a function of the number of neighboring grains. If five or more of the eight neighbouring cells contain  
243 grains then the grain has probability of entrainment  $p_c$ , otherwise it has probability  $p_i$ . In most model  
244 runs  $p_c$  was set to a value less than that of  $p_i$ , thus accounting for the impact of sediment cover in  
245 decreasing local shear stress (though increased flow resistance) and increasing the critical  
246 entrainment shear stress for grains (via lower grain exposure and increased pivot angles). Thus, in  
247 the model, grain scale dynamics of entrainment are varied by adjusting the values of  $p_i$  and  $p_c$ . This  
248 has a direct effect on the reach-scale distribution of cover, which is captured by our  $P$ -function (eq.  
249 3).

250  
251 The model is run with a domain that is 100 cells wide by 1000 cells long, with each cell having the  
252 same area as a grain. Up to four grains can potentially be entrained from each cell in a time step,  
253 limiting the maximum sediment flux. In each time step random numbers and the probabilities are  
254 used to select the grains that are entrained, which are then moved a step length downstream. A  
255 fixed number of grains are also supplied to the upstream end of the model domain. A smoothing  
256 algorithm is applied to prevent unrealistically tall piles of grains developing in cells if there are far  
257 fewer grains in adjacent cells. After around 500 time steps the model typically reaches a steady state  
258 condition in which the number of grains supplied to and leaving the model domain are equal.  
259 Sediment cover is measured in a downstream area of the model domain and is defined as grains that  
260 are not entrained in a given time step. Consequently grains that are deposited in one time step, and  
261 entrained in the following one do not contribute to the sediment cover, and so the model implicitly  
262 incorporates the effect of local sediment cover on grain deposition.

263  
264 Model runs were completed with a six different combinations of  $P_i$  and  $P_c$ : 0.95/0.95, 0.95/0.75,  
265 0.75/0.10, 0.75/0.30, 0.30/0.30 and 0.95/0.05. These combinations were selected to cover the range  
266 of relationships between relative sediment supply  $Q_s^*$  and the exposed bed fraction  $A^*$  observed by  
267 Hodge and Hoey (2012). For each pair of  $P_i$  and  $P_c$  model runs were completed at least 20 different  
268 values of  $Q_s^*$  in order to quantify the model behaviour.

269  
270 Cover bed fraction and total mass on the bed given out by the model were converted using eq. (3)  
271 into the probabilistic framework (Fig. 3). The derivative was approximated by simple linear finite  
272 differences, which, in the case of run-away alluviation, resulted in a non-continuous curve due to  
273 large gradients. The exponential benchmark (eq. 9) is also shown for comparison. The different  
274 model parameterisations produce results in which the probability of deposition on bedrock is both  
275 more and less likely than in the baseline case, with some runs showing both behaviours. Cases where  
276 the probability is more than the baseline case (i.e. grains are more likely to fall on uncovered areas)  
277 are associated with runs in which grains in clusters are relatively immobile. These runs are likely to be  
278 particularly affected by the smoothing algorithm that acts to move sediment from alluviated to  
279 bedrock areas. All model parameterisations predict greater bed exposure for a given normalised  
280 mass than is predicted by a linear cover relationship (Figure 3b). Runs with relatively more immobile  
281 cluster grains have a lower exposed fraction for the same normalised mass. Runs with low values of  
282  $P_i$  and  $P_c$  seem to lead to behavior in which cover is more likely than in the exponential benchmark,  
283 while for high values, it is less likely. However, there are complex interactions and general  
284 statements cannot be made straightforwardly.



286  
287 Fig. 3: Probability functions  $P$  and cover function derived from data obtained from the model of  
288 Hodge and Hoey (2012). The grey dashed line shows the exponential benchmark behavior. Grey  
289 shading depicts the area where the cover function cannot run due to conservation of mass. The  
290 legend gives values of the probabilities of entrainment  $P$  and  $P_c$  used for the runs (see text).

291

292

### 293 3. Cover development in time and space

294

#### 295 3.1. Model derivation

296

297 Previous descriptions of the cover effect relate the exposed fraction of the bed to the relative  
298 sediment supply  $Q_s^*$  (see eqs. 1 and 2). The relation between  $Q_s^*$  and  $M_s$ , which we used in eq. (3),  
299 has often been muddled and incorrect (see, for example, Turowski et al., 2007). In this chapter, we  
300 derive a model to clarify this relationship and put it on a sound physical bases. To this end, the  
301 probabilistic formulation introduced above is extended to allow the calculation of the temporal and  
302 spatial evolution of sediment cover in a stream. Here, we will derive the equations for the one  
303 dimensional case (linear flume), but extensions to higher dimensions are possible in principle. The  
304 derivation is inspired by the erosion-deposition framework (e.g. Charru et al., 2004; Turowski, 2009),  
305 with some necessary adaptions to make it suitable for channels with partial sediment cover. In our  
306 system, we consider two separate mass reservoirs within a control volume. The first reservoir  
307 contains all particles in motion, the total mass per bed area of which is denoted by  $M_m$ , while the  
308 second reservoir contains all particles that are stationary on the bed, the total mass per bed area of  
309 which is denoted by  $M_s$ . We need then three further equations, one to connect the rate of change of  
310 mobile mass to the sediment flux in the flume, one to govern the exchange of particles between the  
311 two reservoirs, and one to describe how sediment transport rate is related to the mobile mass. The  
312 first of these is of course the Exner equation of sediment continuity (e.g. Paola and Voller, 2005),  
313 which captures mass conservation in the system. Instead of the common approach tracking the  
314 height of the sediment over a reference level, we use the total sediment mass on the bed as a  
315 variable, giving

316

$$317 \frac{\partial M_m}{\partial t} = -\frac{\partial q_s}{\partial x} + E - D$$

318 (eq. 13)

319 Here,  $x$  is the coordinate in the streamwise direction,  $t$  the time,  $q_s$  the sediment mass transport rate  
320 per unit width, while  $E$  is the mass entrainment rate per bed area and  $D$  is the mass deposition rate  
321 per bed area. The latter two terms describe the exchange of particles between reservoirs; in the  
322 single reservoir Exner equation these terms are not needed. It is clear that for the problem at hand

323 the choice of total mass or volume as a variable to track the amount of sediment in the reach of  
 324 interest is preferable to the height of the alluvial cover, since necessarily, when cover is patchy, the  
 325 height of the alluvium varies across the bed. It is useful to work with dimensionless variables by  
 326 defining  $t^* = t/T$  and  $x^* = x/L$ , where  $T$  and  $L$  are suitable time and length scales, respectively. The  
 327 dimensionless mobile mass per bed area  $M_m^*$  is equal to  $M_m/M_0$ , and eq. (13) becomes:

328

$$329 \quad \frac{\partial M_m^*}{\partial t^*} = -\frac{\partial q_s^*}{\partial x^*} + E^* - D^*$$

330 (eq. 14)

331 Here,

332

$$q_s^* = \frac{T}{LM_0} q_s$$

333 (eq. 15)

334 The dimensionless entrainment and deposition rates,  $E^*$  and  $D^*$ , are equal to  $TE/M_0$  and  $TD/M_0$ ,  
 335 respectively. The rate of change of the stationary sediment mass  $M_s$  in time is the difference of the  
 336 deposition rate  $D$  and the entrainment rate  $E$ :

337

338

$$\frac{\partial M_s}{\partial t} = D - E$$

339 (eq. 16)

340 Or, using dimensionless variables

341

$$\frac{\partial M_s^*}{\partial t^*} = D^* - E^*$$

342 (eq. 17)

343 We also need sediment entrainment and deposition functions. The entrainment rate needs to be  
 344 modulated by the availability of sediment on the bed. If  $M_s^*$  is equal to zero, no material can be  
 345 entrained. A plausible assumption is that the maximal entrainment rate,  $E_{max}^*$ , is equal to the  
 346 transport capacity.

347

$$E_{max}^* = q_t^*$$

348 (eq. 18)

349 Here,  $q_t^*$  is the dimensionless mass transport capacity, which is related to the transport capacity per  
 350 unit width  $q_t$  by a relation similar to eq. (15). To first order, the rate of change in entrainment rate,  
 351  $dE$ , is proportional to the difference of  $E_{max}$  and  $E$ , and to the rate of change in mass on the bed.

352

353

$$dE^* = (E_{max}^* - E^*)dM_s^* = (q_t^* - E^*)dM_s^*$$

354 (eq. 19)

355 Integrating, we obtain

356

357

$$E^* = E_{max}^* (1 - e^{-M_s^*}) = (1 - e^{-M_s^*})q_t^*$$

358 (eq. 20)

359 Here, we used the condition  $E^*(M_s^* = 0) = 0$  to fix the integration constant to  $E_{max}^*$ . As required, eq.  
 360 (20) approaches  $E_{max}^*$  as  $M_s^*$  goes to infinity, and is equal to zero when  $M_s^*$  is equal to zero. Using a  
 361 similar line of argument, and by assuming the maximum deposition rate to be equal to  $q_s^*$ , we arrive  
 362 at an equation for the deposition rate  $D^*$ .

363

364

$$D^* = (1 - e^{-M_m^*})q_s^*$$

365 (eq. 21)

366 When  $M_m^*$  is small, then the amount that can be deposited is limited by  $M_m^*$ . If  $M_m^*$  is large, then  
 367 deposition is limited by sediment supply. Substituting eqs. (20) and (21) into eq. (17), we obtain:

368

$$369 \quad \frac{\partial M_s^*(x^*, t^*)}{\partial t^*} = D^* - E^* = (1 - e^{-M_m^*(x^*, t^*)})q_s^*(x^*, t^*) - (1 - e^{-M_s^*(x^*, t^*)})q_t^*(x^*, t^*)$$

370 (eq. 22)

371 Note that  $q_s^*/q_t^* = Q_s^*$ . The equation for the mobile mass (eq. 14) becomes:

372

$$373 \quad \frac{\partial M_m^*(x^*, t^*)}{\partial t^*} = -\frac{\partial q_s^*}{\partial x^*} - (1 - e^{-M_m^*(x^*, t^*)})q_s^*(x^*, t^*) + (1 - e^{-M_s^*(x^*, t^*)})q_t^*(x^*, t^*)$$

374 (eq. 23)

375 Finally, the sediment transport rate needs to be proportional to the mobile sediment mass times the  
376 downstream sediment speed  $U$ , and we can write

377

$$378 \quad q_s^*(x^*, t^*) = U^*(x^*, t^*)M_m^*(x^*, t^*)$$

379 (eq. 24)

380 Here

$$381 \quad U^* = \frac{T}{L}U$$

382 (eq. 25)

383

384 After incorporating the original equation between  $A^*$  and  $M_s^*$  (eq. 3), the system of four differential  
385 equations (3), (22), (23) and (24) contains four unknowns: the downstream gradient in the sediment  
386 transport rate  $\partial q_s^*/\partial x^*$ , the exposed fraction of the bed  $A^*$ , the non-dimensional stationary mass  $M_s^*$ ,  
387 and the non-dimensional mobile mass  $M_m^*$ , while the non-dimensional transport capacity  $q_t^*$  and the  
388 non-dimensional downstream sediment speed  $U^*$  are input variables, and  $P$  is a externally specified  
389 function. In addition, sediment input  $q_s^*$  needs to be specified as an upstream boundary condition  
390 and initial values for the mobile mass  $M_m^*$  and the stationary mass  $M_s^*$  need to be specified  
391 everywhere.

392

393 **3.2. Time-independent solution**

394

395 Setting the time derivatives to zero, we obtain a time-independent solution, which links the exposed  
396 area directly to the ratio of sediment transport rate to transport capacity. From eq. (23) it follows  
397 that in this case, the entrainment rate is equal to the deposition rate and we obtain

$$398 \quad (1 - e^{-\bar{M}_m^*})\bar{q}_s^* = (1 - e^{-\bar{M}_s^*})\bar{q}_t^*$$

399 (eq. 26)

400 Here, the bar over the variables denotes their steady state value. Substituting eq. (24) to eliminate  
401  $\bar{M}_m^*$  and solving for  $\bar{M}_s^*$  gives

402

$$403 \quad \bar{M}_s^* = -\ln \left\{ 1 - \left( 1 - e^{-\bar{q}_s^*/U^*} \right) \frac{\bar{q}_s^*}{\bar{q}_t^*} \right\} = -\ln \left\{ 1 - \left( 1 - e^{-\frac{\bar{q}_t^* \bar{q}_s^*}{U^* \bar{q}_s^*}} \right) \bar{q}_s^* \right\}$$

404 (eq. 27)

405 Note that we assume here that sediment cover is only dependent on the stationary sediment mass  
406 on the bed and we thus neglect grain-grain interactions known as the dynamic cover (Turowski et al.,  
407 2007). In analogy to eq. (24), we can write

408

$$q_t^* = U^* M_0^*$$

409 (eq. 28)

410 Here,  $M_0^*$  is a characteristic dimensionless mass that depends on hydraulics and therefore implicitly  
411 on transport capacity (which is independent of and should not be confused with the minimum mass

412 necessary to fully cover the bed  $M_0$ ). When sediment transport rate equals transport capacity, then  
 413  $M_0^*$  is equal to the mobile mass of sediment normalized by the reference mass  $M_0$ . It can be viewed  
 414 as a proxy for the transport capacity and is a convenient parameter to simplify the equations. The  
 415 mobile mass can then, in general, be written as follows (cf. Turowski et al., 2007), remembering that  
 416 the relative sediment supply  $Q_s^* = 1$  when supply is equal to capacity:

$$417 \quad M_m^* = M_0^* Q_s^*$$

418 (eq. 29)

419 If we use the exponential cover function (eq. 9) with eqs. (27), (28) and (29) we obtain

420

$$421 \quad \bar{A}^* = 1 - \left(1 - e^{-\bar{q}_s^*/U^*}\right) \frac{\bar{q}_s^*}{\bar{q}_t^*} = 1 - \left(1 - e^{-\frac{\bar{q}_t^* \bar{Q}_s^*}{U^*}}\right) \bar{Q}_s^* = 1 - \left(1 - e^{-M_0^* \bar{Q}_s^*}\right) \bar{Q}_s^*$$

422 (eq. 30)

423 Similarly, equations can be found for the other analytical solutions of the cover function. For the  
 424 linear case (eq. 7), we obtain:

$$425 \quad \bar{A}^* = 1 + \ln \left\{ 1 - \left(1 - e^{-M_0^* \bar{Q}_s^*}\right) \bar{Q}_s^* \right\}$$

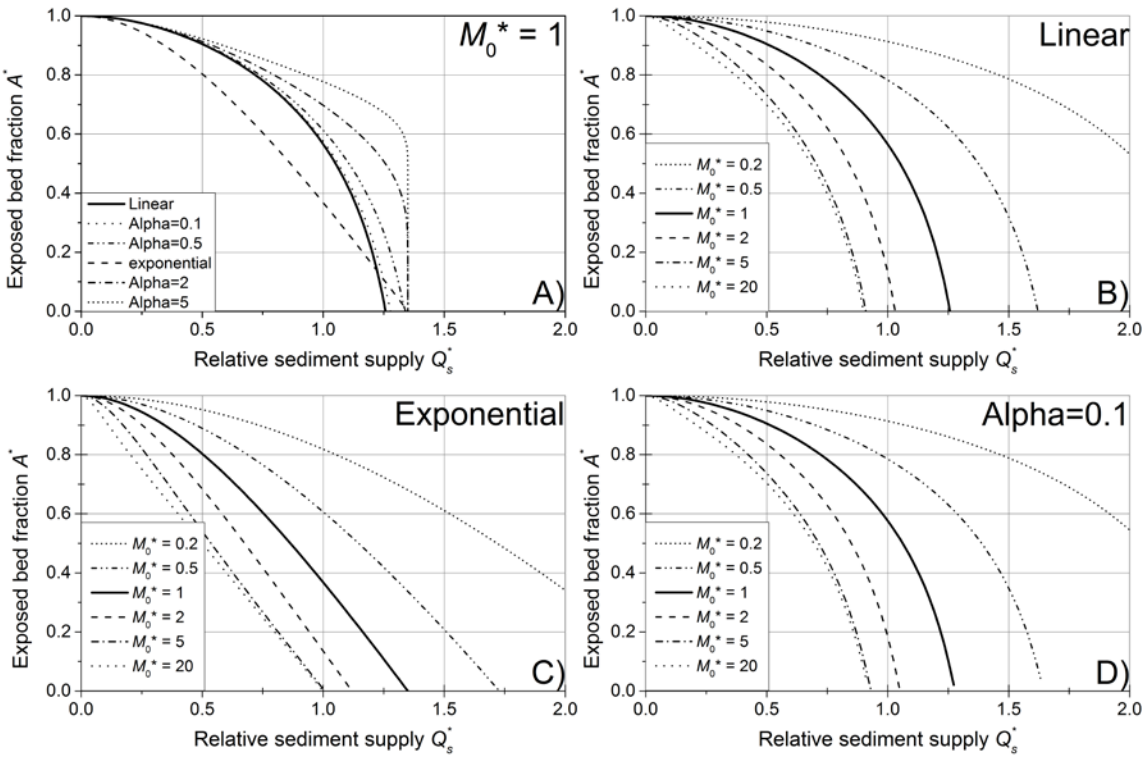
426 (eq. 31)

427 For the power law case (eq. 10), we obtain:

$$428 \quad \bar{A}^* = \left[ 1 + (1 - \alpha) \ln \left\{ 1 - \left(1 - e^{-M_0^* \bar{Q}_s^*}\right) \bar{Q}_s^* \right\} \right]^{\frac{1}{1-\alpha}}$$

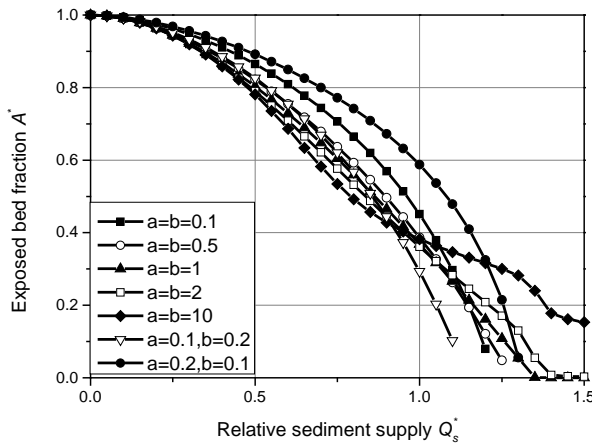
429 (eq. 32)

430 It is interesting that the assumption of an exponential cover function essentially leads to a combined  
 431 linear and exponential relation between  $\bar{A}^*$  and  $\bar{Q}_s^*$ . Instead of a linear decline as the original linear  
 432 cover model, or a concave-up relationship as the original exponential model, the function is convex-  
 433 up for all solutions (Fig. 4). Adjusting  $M_0^*$  shifts the lines: decreasing  $M_0^*$  leads to a delayed onset of  
 434 cover and vice versa. The former result arises because a lower  $M_0^*$  means that the sediment flux is  
 435 conveyed through a smaller mass moving at a higher velocity. The original linear cover function (eq.  
 436 1) can be recovered from the exponential model with a high value of  $M_0^*$ , since the exponential term  
 437 quickly becomes negligible with increasing  $\bar{Q}_s^*$  and the linear term dominates (Fig. 4C). Note that for  
 438 the linear (eq. 6) and the power law cases (eq. 10), high values of  $M_0^*$  may give  $\bar{A}^* = 0$  for  $\bar{Q}_s^* < 1$  (Fig.  
 439 4B,D), which is consistent with the concept of runaway alluviation. Using the beta distribution to  
 440 describe  $P$ , a numerical solution is necessary, but a wide range of steady-state cover functions can be  
 441 obtained (Fig. 5). By varying the value of  $M_0^*$ , an even wider range of behavior can be obtained.



442  
 443  
 444  
 445  
 446  
 447

Fig. 4: Analytical solutions at steady state for the exposed fraction of the bed ( $A^*$ ) as a function of relative sediment supply ( $Q_s^*$ , cf. Fig. 1). A) Comparison of the different solutions, keeping  $M_0^*$  constant at 1. B) Varying  $M_0^*$  for the linear case (eq. 31). C) Varying  $M_0^*$  for the exponential case (eq. 30). D) Varying  $M_0^*$  for the power law case with  $\alpha = 0.1$  (eq. 32).



448  
 449  
 450  
 451  
 452  
 453  
 454  
 455

Fig. 5: Steady state solutions using the beta distribution to parameterize  $P$  (eq. 11) for a range of parameters  $a$  and  $b$ , and using  $M_0^* = 1$  (cf. Fig. 2). The solutions were obtained by iterating the equations to a steady state, using initial conditions of  $A^* = 1$  and  $M_m^* = M_s^* = 0$ .

The previous analysis shows that steady state cover is controlled by the characteristic dimensionless mass  $M_0^*$ , which is equal to the ratio of dimensionless transport capacity and particle speed (eq. 28). Converting to dimensional variables, we can write

456 
$$M_0^* = \frac{q_t^*}{U^*} = \frac{q_t}{M_0 U}$$

457 (eq. 33)

458 The minimum mass necessary to completely cover the bed per unit area,  $M_0$ , can be estimated  
459 assuming a single layer of close-packed spherical grains residing on the bed (cf. Turowski, 2009),  
460 giving:

461 
$$M_0 = \frac{\pi \rho_s D_{50}}{3\sqrt{3}}$$

462 (eq. 34)

463 Here,  $\rho_s$  is the sediment density and  $D_{50}$  is the median grain size. We use equations derived by  
464 Fernandez-Luque and van Beek (1976) from flume experiments that describe transport capacity and  
465 particle speed as a function of bed shear stress (see also Lajeunesse et al., 2010, and Meyer-Peter  
466 and Mueller, 1948, for similar equations):

467

468 
$$q_t = 5.7 \frac{\rho_s \rho}{(\rho_s - \rho) g} \left( \frac{\tau}{\rho} - \frac{\tau_c}{\rho} \right)^{3/2}$$

469 (eq. 35)

470

471 
$$U = 11.5 \left( \left( \frac{\tau}{\rho} \right)^{1/2} - 0.7 \left( \frac{\tau_c}{\rho} \right)^{1/2} \right)$$

472 (eq. 36)

473 Here,  $\tau_c$  is the critical bed shear stress for the onset of bedload motion,  $g$  is the acceleration due to  
474 gravity and  $\rho$  is the water density. Combining eqs. (34), (35) and (36) to get an equation for  $M_0^*$  gives:

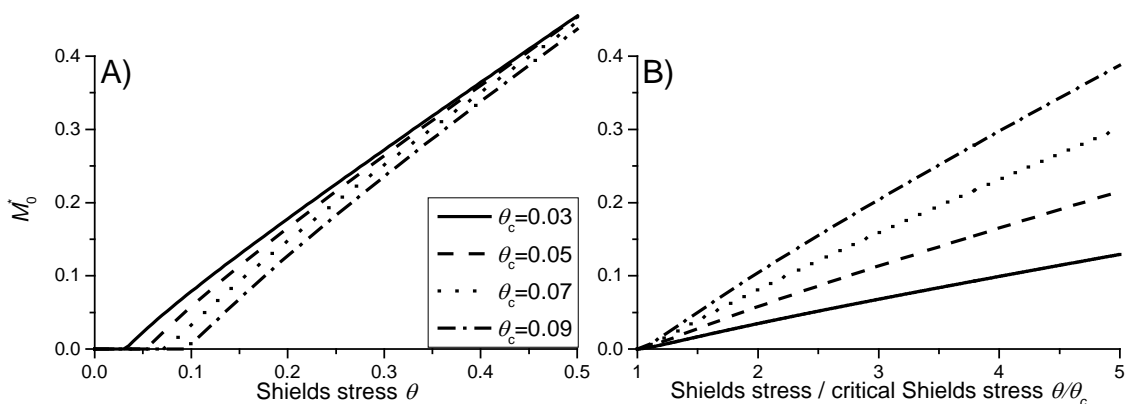
475

476 
$$M_0^* = \frac{3\sqrt{3}}{2\pi} \frac{(\theta - \theta_c)^{3/2}}{\theta^{1/2} - 0.7\theta_c^{1/2}} = \frac{3\sqrt{3}\theta_c}{2\pi} \frac{(\theta/\theta_c - 1)^{3/2}}{(\theta/\theta_c)^{1/2} - 0.7}$$

477 (eq. 37)

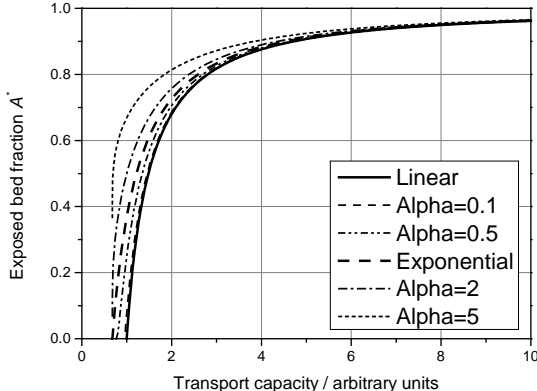
478 Here, the Shields stress  $\theta = \tau/(\rho_s - \rho)gD_{50}$ , and  $\theta_c$  is the corresponding critical Shields stress, and we  
479 approximated  $5.7/11.5 = 0.496$  with  $1/2$  (compare to eqs. 35/36). At high  $\theta$ , when the threshold can  
480 be neglected, eq. (37) reduces to a linear relationship between  $M_0^*$  and  $\theta$ . Near the threshold,  $M_0^*$  is  
481 shifted to lower values as  $\theta_c$  increases (Fig. 6). The systematic variation of  $U^*$  with the hydraulic  
482 driving conditions (eq. 36) implies that the cover function evolves differently in response to changes  
483 in sediment supply and transport capacity. For a first impression, by comparing equations (35) and  
484 (36), we assume that particle speed scales with transport capacity raised to the power of one third  
485 (Fig. 7).

486



487

488 Fig. 6: The characteristic dimensionless mass  $M_0^*$  depicted as a function of A) the Shields stress and  
 489 B) the ratio of Shields stress to critical Shields stress (eq. 37).  
 490



491  
 492 Fig. 7: Variation of the exposed bed fraction as a function of transport capacity, assuming that  
 493 particle speed scales with transport capacity to the power of one third.

494  
 495 **3.3 Temporal evolution of cover within a reach**  
 496 *3.3.1 System timescales*

497 To calculate the temporal evolution of cover on the bed within a single reach, we solved the  
 498 equations numerically for a section of the bed with homogenous conditions using a simple linear  
 499 finite difference scheme. Then, the sediment input is a boundary condition, while sediment output,  
 500 mobile and stationary sediment mass and the fraction of the exposed bed are output variables. In  
 501 general, a change in sediment supply leads to a gradual adjustment of the output variables towards a  
 502 new steady state (Fig. 8). Unfortunately, a general analytical solution is not possible, but a result can  
 503 be obtained for the special case of  $q_s^* = 0$ . Such a situation is rare in nature, but could be easily  
 504 created in flume experiments as a model test. Then, the time derivative of stationary mass is given  
 505 by:

506

$$507 \frac{\partial M_s^*}{\partial t^*} = -(1 - e^{-M_s^*}) q_t^*$$

508 (eq. 38)  
 509 Using the exponential cover model (eq. 9), we obtain:

510

$$511 \frac{1}{A^*(1 - A^*)} \frac{\partial A^*}{\partial t^*} = q_t^*$$

512 (eq. 39)  
 513 Equation (39) is separable and can be integrated to obtain

514

$$515 \ln(A^*) - \ln(1 - A^*) = t^* q_t^* + C$$

516 (eq. 40)  
 517 Letting  $A^*(t^*=0) = A^*_0$ , where  $A^*_0$  is the initial cover, the final equation is

518

$$519 \frac{1 - A^*}{1 - A_0^*} \frac{A_0^*}{A^*} = e^{-t^* q_t^*}$$

520 (eq. 41)  
 521 To clarify the characteristic time scale of the process, equation (41) can also be written in the form of  
 522 a sigmoidal-type function:

523

524

$$A^* = \frac{1}{1 + \left(\frac{1 - A_0^*}{A_0^*}\right) e^{-t^* q_t^*}}$$

525 (eq. 42)

526 By making the parameters in the exponent on the right hand side of eq. (42) dimensional, we get:

527

528

$$t^* q_t^* = \frac{t}{T} \frac{T}{LM_0} q_t = \frac{t q_t}{LM_0}$$

529 (eq. 43)

530 which allows a characteristic system time scale  $T_E$  to be defined as

531

$$T_E = \frac{LM_0}{q_t}$$

532 (eq. 44)

533 Since this time scale is dependent on the transport capacity  $q_t$ , we can view it as a time scale  
 534 associated with the entrainment of sediment from the bed (cf. eq. 20) – hence the subscript  $E$  on  $T_E$ .  
 535 From eq. (42), the exposed bed fraction evolves in an asymptotic fashion towards equilibrium (Fig. 9).  
 536 We can expect that there are other characteristic time scales for the system, for example associated  
 537 with sediment deposition or downstream sediment evacuation.

538

539 We can make some further progress and define a more general system time scale by performing a  
 540 perturbation analysis (Appendix A). For small perturbations in either  $q_s^*$  or  $q_t^*$ , we obtain an  
 541 exponential term describing the transient evolution, which allows the definition of a system  
 542 timescale  $T_S$

543

$$\exp \left\{ - \left( \bar{q}_t^* - \left( 1 - e^{-\bar{q}_s^*/\bar{U}^*} \right) \bar{q}_s^* \right) t^* \right\} = \exp \left\{ - \frac{t}{T_S} \right\}$$

544 (eq. 45)

545 The characteristic system time scale can then be written as

546

$$T_S = \frac{LM_0}{\bar{q}_t \left( 1 - \left( 1 - e^{-\bar{q}_s^*/\bar{U}^*} \right) \bar{q}_s^* \right)} = \frac{LM_0}{\bar{q}_t} e^{\bar{M}_s^*}$$

547 (eq. 46)

548 Note that for  $q_s^* = 0$ , eq. (46) reduces to eq. (44), as would be expected. Since  $\bar{M}_s^*$  is directly related  
 549 to steady state bed exposure  $\bar{A}^*$ , we can rewrite the equation, for example by assuming the  
 550 exponential cover function (eq. 3), as

551

$$T_S = \frac{LM_0}{\bar{q}_t \bar{A}^*}$$

552 (eq. 47)

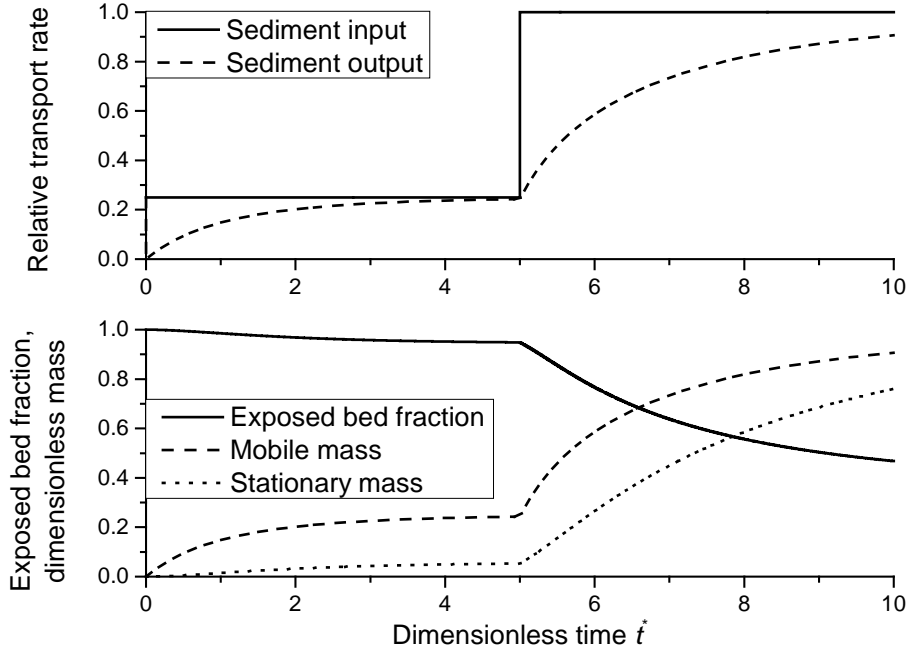
553 Since bed cover is more easily measurable than the mass on the bed, eq. (47) can help to estimate  
 554 system time scales in the field. Further,  $\bar{A}^*$  varies between 0 and 1, which allows estimating a  
 555 minimum system time using eq. (44). As  $\bar{A}^*$  approaches zero, the system time scale diverges.

556

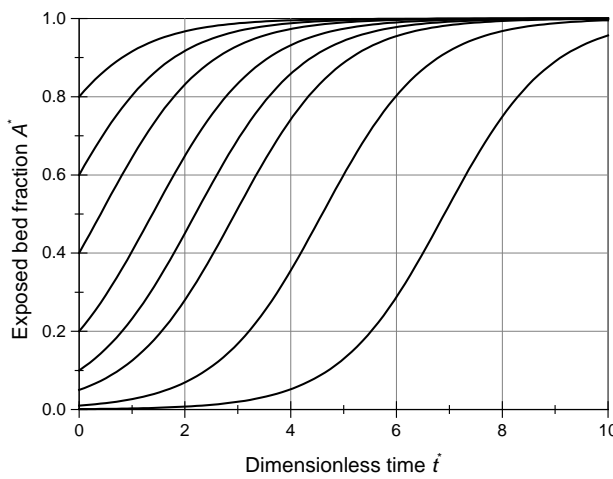
557 To illustrate these additional dependencies, we have used numerical solutions of eqs. (3), (22), (23)  
 558 and (24) to calculate the time needed to reach 99.9% of total adjustment after a step change in  
 559 transport stage (chosen due to the asymptotic behavior of the system), produced by varying particle  
 560 speed  $U$  over a range of plausible values (Fig. 10). Response time decreases as particle speed  
 561 increases. This reflects elevated downstream evacuation for higher particles speeds, resulting in a  
 562 smaller mobile particle mass and thus higher entrainment and lower deposition rates. Response time

563 also increases with increasing relative sediment supply  $Q_s^*$ . As the runs start with zero sediment  
 564 cover, and the extent of cover increases with  $Q_s^*$ , at higher  $Q_s^*$  the adjusted cover takes longer to  
 565 develop.

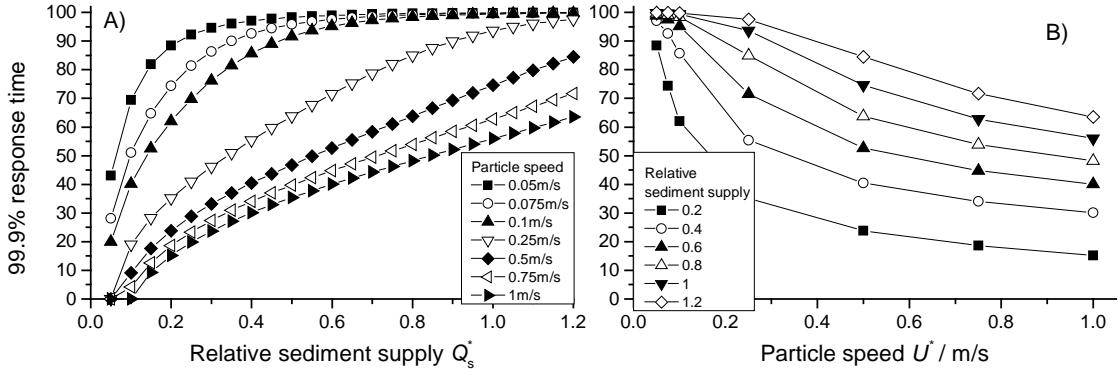
566



567  
 568 Fig. 8: Temporal evolution of cover for the simple case of a control box with sediment through-flux,  
 569 based on eqs. (3), (22), (23) and (24). Relative sediment supply (supply normalized by transport  
 570 capacity) was specified to 0.25 and increased to 1 at  $t^* = 5$ . The response of sediment output, mobile  
 571 and stationary sediment mass and the exposed bed fraction was calculated. Here, we used the  
 572 exponential function for  $P$  (eq. 9) and  $M_0^* = U^* = 1$ . The initial values were  $A^* = 1$  and  $M_m^* = M_s^* = 0$ .  
 573



574  
 575 Fig. 9: Evolution of the exposed bed fraction (removal of sediment cover) over time starting with  
 576 different initial values of bed exposure, for the special case of no sediment supply, i.e.,  $q_s^* = 0$  (eq. 41)  
 577 and  $q_t^* = 1$ .  
 578



579

580 Fig. 10: Dimensionless time to reach 99.9% of the total adjustment in exposed area as a function of  
 581 A) transport stage and B) particle speed. All simulation were started with  $A^* = 1$  and  $M_m^* = M_s^* = 0$ .

582

583

### 584 3.3.2 Phase shift and gain in response to a cyclic perturbation

585 The perturbation analysis (Appendix A) gives some insight into the response of cover to cyclic  
 586 sinusoidal perturbations. Let sediment supply be perturbed in a cyclic way described by an equation  
 587 of the form

$$588 q_s^* = \bar{q}_s^* + \delta q_s^* = \bar{q}_s^* + d \sin\left(\frac{2\pi t}{p}\right)$$

589 (eq. 48)

590 Here, the overbar denotes the temporal average,  $\delta q_s^*$  is the time-dependent perturbation,  $d$  is the  
 591 amplitude of the perturbation and  $p$  its period. A similar perturbation can be applied to the transport  
 592 capacity (see Appendix A). The reaction of the stationary mass and therefore cover can then also be  
 593 described by sinusoidal function of the form (Appendix A)

$$594 \delta M_s^* = G \sin\left(\frac{2\pi t}{p} + \varphi\right)$$

595 (eq. 49)

596 Here,  $\delta M_s^*$  is the perturbation of the stationary sediment mass around the temporal average,  $G$  is  
 597 known as the gain, describing the amplitude response, and  $\varphi$  is the phase shift. If the gain is large,  
 598 stationary mass reacts strongly to the perturbation; if it is small, the forcing does not leave a signal.  
 599 The phase shift is negative if the response lags behind the forcing and positive if it leads. The phase  
 600 shift can be written as

$$601 \varphi = \tan^{-1}\left(-2\pi \frac{T_s}{p}\right)$$

602 (eq. 50)

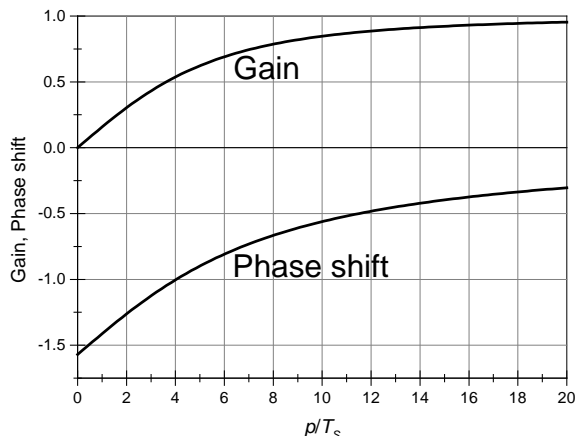
603 The gain can be written as

$$604 G = \frac{p}{T_s} \frac{Kd}{\sqrt{\left(\frac{p}{T_s}\right)^2 + 4\pi^2}}$$

605 (eq. 51)

606 Here,  $d$  is the amplitude of the perturbation, and  $K$  is a function of the time-averaged values of  $q_s$ ,  $q_t$   
 607 and  $U$  and differs for perturbations in transport capacity and sediment supply (see Appendix A).  
 608 Thus, the system behavior can be interpreted as a function of the ratio of the period of perturbation  
 609  $p$  and the system time scale  $T_s$ . The period  $p$  is large if the forcing parameter, i.e., discharge or  
 610 sediment supply, varies slowly and small when it varies quickly. According to eq. (50), the phase shift  
 611 is equal to  $-\pi/2$  for low values of  $p/T_s$  (quickly-varying forcing parameter), implying a substantial lag in  
 612 the adjustment of cover. The phase shift tends to zero as  $p/T_s$  tends to infinity (Fig. 11). The gain

613 varies approximately linearly with  $p/T_s$  for small  $p/T_s$  (quickly-varying forcing parameter), while it is  
 614 approximately constant at a value of  $Kd$  for large  $p/T_s$  (slowly-varying forcing parameter) (eq. 51).  
 615 Thus, if the forcing parameter varies slowly, cover adjustment keeps up at all times.  
 616



617  
 618 Fig. 11: Phase shift (eq. 50) and gain (eq. 51) as a function of the ratio of the period of perturbation  $p$   
 619 and the system time scale  $T_s$ . For the calculation, the constant factor in the gain ( $Kd$ ) was set equal to  
 620 one.

621  
 622 *3.3.3 A flood at the Erlenbach*  
 623 To illustrate the magnitude of the timescales using real data, we use a flood dataset from the  
 624 Erlenbach, a sediment transport observatory in the Swiss Prealps (e.g., Beer et al., 2015). There, near  
 625 a discharge gauge, bedload transport rates are measured at 1-minute resolution using the Swiss Plate  
 626 Geophone System, a highly developed and fully calibrated surrogate bedload measuring system (e.g.,  
 627 Rickenmann et al., 2012; Wyss et al. 2016). We use data from a flood on 20<sup>th</sup> June 2007 (Turowski et  
 628 al., 2009) with highest peak discharge that has so far been observed at the Erlenbach. The  
 629 meteorological conditions that triggered this flood and its geomorphic effects have been described in  
 630 detail elsewhere (Molnar et al., 2010; Turowski et al., 2009, 2013). The Erlenbach does not have a  
 631 bedrock bed in the sense that bedrock is exposed in the channel bed, however, the data provide a  
 632 realistic natural time series of discharge and bedload transport over the course of a single event.  
 633 Rather than predicting bed cover evolution for a natural system, for which we do not currently have  
 634 data for validation, we use the Erlenbach data to illustrate possible cover behavior during a fictitious  
 635 event with different initial sediment cover extents, using natural data to provide realistic boundary  
 636 conditions.

637  
 638 Using a median grain size of 80 mm, a sediment density of 2650 kg/m<sup>3</sup> and a reach length of 50 m,  
 639 we obtained  $M_0 = 128$  kg/m<sup>2</sup>. We calculated transport capacity using the equation of Fernandez  
 640 Luque and van Beek (1976). However, it is known that this and similar equations strongly  
 641 overestimate measured transport rates in streams such as the Erlenbach (e.g., Nitsche et al., 2011).  
 642 Consequently, we rescaled by setting the ratio of bedload supply to capacity to one at the highest  
 643 discharge. The exposed fraction was then calculated iteratively assuming  $P = A^*$  (i.e., the exponential  
 644 cover formulation, eq. 9). In a real flood event, water discharge and sediment supply obviously do  
 645 not follow a small cyclic perturbation (Fig. 11). But we can tentatively relate the observations to the  
 646 theory by assuming that at each time step, the change in sediment supply can be represented by the  
 647 commencement of a sinusoidal perturbation with varying period. To estimate the effective period  $p$ ,  
 648 one needs to take the derivatives of eq. (48).

649 
$$\frac{dq_s^*}{dt} = \frac{d\delta q_s^*}{dt} = \frac{2\pi d}{p} \cos\left(\frac{2\pi t}{p}\right)$$

650 (eq. 52)

651 Setting  $t = 0$  for the time of interest, we can relate  $p$  to the local gradient in bedload supply, which  
652 can be measured from the data.

653

654 
$$\frac{2\pi d}{p} = \frac{\Delta q_s^*}{\Delta t}$$

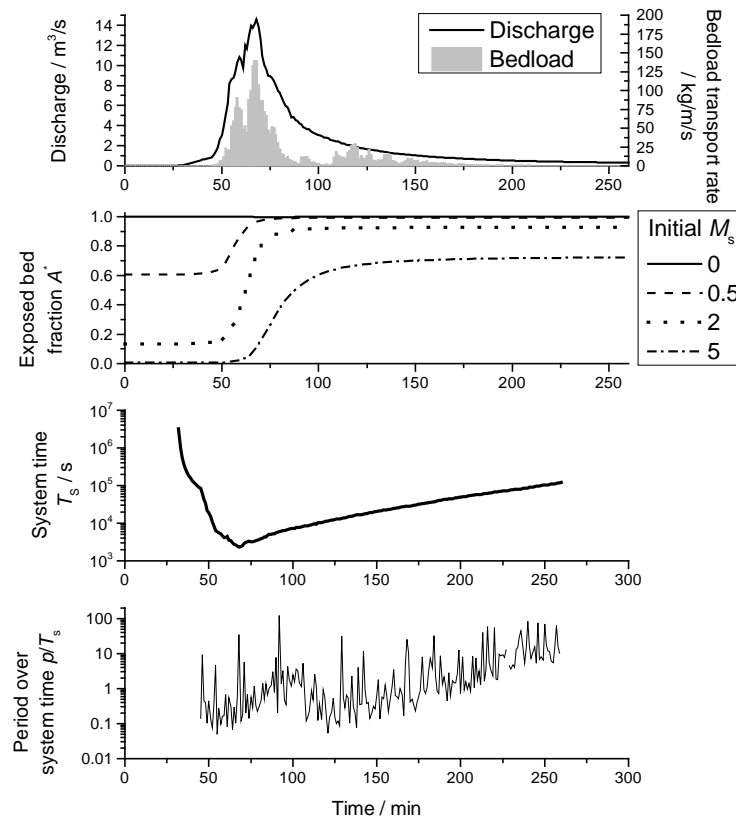
655 (eq. 52)

656 Assuming that all change in the response time is due to changes in the period (i.e., assuming a  
657 constant amplitude,  $d = 1$ ), we can obtain a conservative estimate of the range over which  $p$  varies  
658 over the course of an event.

659 
$$p = 2\pi \frac{\Delta t}{\Delta q_s^*}$$

660 (eq. 52)

661 In the exemplary event, the evolution and final value of bed cover depends strongly on its initial  
662 value (Fig. 12), indicating that the adjustment is incomplete. The system timescale is generally larger  
663 than 1000s and is inversely related to discharge via the dependence on transport capacity. The  
664  $p/T_s$  ratio varies around one, with low values at the beginning of the flood and large values in the  
665 waning hydrograph. Both the high values of the system time scale and the smooth evolution of bed  
666 cover over the course of the flood imply that cover development cannot keep up with the variation in  
667 the forcing characteristics. This dynamic adjustment of cover, which can lag forcing processes, may  
668 thus play an important role in the dynamics of bedrock channels and probably needs to be taken into  
669 account in modelling.



670

671 Fig. 12: Calculated evolution of cover during the largest event observed at the Erlenbach on 20<sup>th</sup> June  
672 2007 (Turowski et al., 2009). Bedload transport rates were measured with the Swiss Plate geophone  
673 sensors calibrated with direct bedload samples (Rickenmann et al., 2012). The final fraction of  
674 exposed bedrock is strongly dependent on its initial value.  
675

#### 676 4. Discussion

##### 677 4.1 Model formulation

678 In principle, the framework for the cover effect presented here allows the formulation of a general  
679 model for bedrock channel morphodynamics without the restrictions of previous models (e.g. Nelson  
680 and Seminara, 2011; Zhang et al., 2015). To achieve this, the dependency of  $P$  on various control  
681 parameters needs to be specified. In general,  $P$  should be controlled by local topography, grain size  
682 and shape, hydraulic forcing, and the amount of sediment already residing on the bed. Furthermore,  
683 the shape of the  $P$  function should also be affected by feedbacks between these properties, such as  
684 the development of sediment cover altering the local roughness and hence altering hydraulics and  
685 local transport capacity (Inoue et al., 2014; Johnson, 2014). Within the treatment presented here, we  
686 have explicitly accounted only for the impact of the amount of sediment already residing on the bed.  
687 However, all of the mentioned effects can be included implicitly by an appropriate choice of  $P$ . The  
688 exact relationships between, say, bed topography and  $P$  need to be mapped out experimentally (e.g.,  
689 Inoue et al., 2014), with theoretical approaches also providing some direction (cf. Johnson, 2014;  
690 Zhang et al., 2015). Currently available experimental results (Chatanantavet and Parker, 2008;  
691 Finnegan et al., 2007; Hodge and Hoey, 2016; Inoue et al., 2014; Johnson and Whipple, 2007) cover  
692 only a small range of the possible parameter space and, in general, not all necessary parameters to  
693 constrain  $P$  were reported. Specifically the stationary mass of sediment residing on the bed is usually  
694 not reported and can be difficult to determine experimentally, but is necessary to determine  $P$ .  
695 Nevertheless, depending on the choice of  $P$ , our model can yield a wide range of cover functions that  
696 encompasses reported functions both from numerical modelling (e.g., Aubert et al., 2016; Hodge and  
697 Hoey, 2012; Johnson, 2014) and experiments (Chatanantavet and Parker, 2008; Inoue et al., 2014;  
698 Sklar and Dietrich, 2001) (see Figs. 4 and 5).  
699

700 The dynamic model put forward here is a minimum first order formulation, and there are some  
701 obvious future alterations. We only take account of the static cover effect caused by immobile  
702 sediment on the bed. The dynamic cover effect, which arises when moving grains interact at high  
703 sediment concentration and thus reduce the number of impacts on the bed (Turowski et al., 2007),  
704 could in principle be included into the formulation, but would necessitate a second probability  
705 function specifically to describe this dynamic cover. It would also be possible to use different  $P$ -  
706 functions for entrainment and deposition, thus introducing hysteresis into cover development. Such  
707 hysteresis has been observed in experiments in which the equilibrium sediment cover was a function  
708 of the initial extent of sediment cover (Chatanantavet and Parker, 2008; Hodge and Hoey, 2012).  
709 Whether such alterations are necessary is best established with targeted laboratory experiments.  
710

##### 711 4.2 Comparison to previous modelling frameworks

712 We will briefly outline in this section the main differences to previous formulations of cover dynamics  
713 in bedrock channels. Thus, the novel aspects of our formulation and the respective advantages and  
714 disadvantages will become clear.

715  
716 Aubert et al. (2015) coupled the movement of spherical particles to the simulation of a turbulent  
717 fluid and investigated how cover depended on transport capacity and supply. Similar to what is  
718 predicted by our analytical formulation, they found a range of cover function for various model set-

ups, including linear and convex-up relationships (compare the results in Fig. 4 to their Fig. 15). Despite short-comings, Aubert et al. (2015) presented the so far most detailed physical simulations of bed cover formation and the correspondence between the predictions is encouraging.

Nelson and Seminara (2011, 2011) formulated a morphodynamic model for bedrock channels. They based their formulation on sediment concentration, which is in principle similar to our formulation based on mass. However, Nelson and Seminara (2011, 2012) did not distinguish between mobile and stationary sediment and linked local transport directly to sediment concentration. Further, a given mass can be distributed in multiple ways to achieve various degrees of cover, a fact that is quantified in our formulation by the probability parameter  $P$ . Nelson and Seminara (2011, 2012) assumed a direct correspondence between sediment concentration and degree of cover, which is equivalent to the linear cover assumption (eq. 7), with the associated problems outlined earlier. Practically, this implies that the grid size needs to be of the order of the grain size. Although different in various details, Inoue et al. (2016) have used essentially the same approach as Nelson and Seminar (2011, 2012) to link bedload concentration, transport and bed cover. Both of these models allow the 2D modelling of bedrock channel morphology. Although we have not fully developed such a model in the present paper, our model framework could easily be extended to 2D problems.

Inoue et al. (2014) formulated a 1D model for cover dynamics and bedrock erosion. There, they distinguish between stationary and mobile sediment using an Exner equation to capture sediment mass conservation. The degree of bed cover is related to transport rates and sediment mass via a saturation volume, which is related to our characteristic mass  $M_0^*$  (see section 3.2). A key difference between Inoue et al.'s (2014) model and the one presented here lies in the sediment continuity equation (eq. 26), in which we explicitly take account of both entrainment and deposition. In addition, with the function  $P$ , describing the relationship between deposited mass and degree of cover, we provide a more flexible framework for complex simulations where the bed needs to be discretized (e.g., 2D models or reach-scale formulations).

Zhang et al. (2015) formulated a bed cover model specifically for beds with macro-roughness. There, deposited sediment always fills topographic lows from their deepest positions, such that there is a reach-uniform sediment level. While the model is interesting and provides a fundamentally different approach to what is suggested here, its applicability is limited to very rough beds and the assumption of a sediment elevation that is independent of the position on the bed seems physically unrealistic. In principle, the probabilistic framework presented here should be able to deal with macro-rough beds as well and thus allows a more general treatment of the problem of bed cover.

Within this paper, we focused on the dynamics of bed cover, rather than modelling the dynamics of entire channels. The probabilistic formulation using the parameter  $P$  provides a flexible framework to connect the sediment mass residing on the bed with the exposed bedrock fraction. This particular element has not been treated in any of the previous models and could be easily implemented in other approaches dealing with sediment fluxes along and across the stream and the interaction with erosion and, over long time scales, channel morphology. However, it is as yet unclear how flow hydraulics, sediment properties and other conditions affect  $P$  and this should be investigated in targeted laboratory experiments. Nevertheless, the proposed formulation provides a framework in which data from various sources can be easily compared and discussed.

#### 765 4.3 Further implications

766 Based on field data interpretation, Phillips and Jerolmack (2016) argued that bedrock rivers adjust  
767 such that, similar to alluvial channels, medium sized floods are most effective in transporting  
768 sediment, and that channel geometry therefore can quickly adjust their transport capacity to the  
769 applied load and therefore achieve grade (cf. Mackin, 1948). They conclude that bedrock channels  
770 can adjust their morphologic parameters (channel width and shape) quickly in response to changing  
771 boundary conditions, a somewhat counter-intuitive notion for slowly-eroding channels. In contrast,  
772 our model suggests that bed cover can be adjusted to achieve grade. In steady state, time derivatives  
773 need to be equal to zero. Thus, entrainment equals deposition (eq. 16), implying that the  
774 downstream gradient in sediment transport rate is equal to zero (eq. 14). When sediment supply or  
775 transport capacity change, the exposed bedrock fraction can adjust to achieve a new steady state  
776 and a change of the channel geometry is unnecessary. These changes in sediment cover can occur far  
777 more rapidly than changes in width and cross-sectional shape (compare to eq. 47). Whether a steady  
778 state is achieved depends on the relative magnitude of the timescales of perturbation and cover  
779 adjustment (see section 3.2). Our results imply that bedrock channels have two distinct time scales to  
780 adjust to changing boundary conditions to achieve grade. Over short times, bed cover is adjusted.  
781 This can occur rapidly. Over long time scales, channel width, cross-sectional shape and slope are  
782 adjusted.  
783

## 784 5. Conclusions

785

786 The probabilistic view put forward in this paper offers a framework into which diverse data on bed  
787 cover, whether obtained from field studies, laboratory experiments or numerical modeling, can be  
788 easily converted to be meaningfully compared. The conversion requires knowledge of the mass of  
789 sediment on the bed and the evolution of exposed fraction of the bed. Within the framework,  
790 individual data sets can be compared to the exponential benchmark and linear limit cases, enabling  
791 physical interpretation. Furthermore, the formulation allows the general dynamic sub-grid modelling  
792 of bed cover. Depending on the choice of  $P$ , the model yields a wide range of possible cover  
793 functions. Which of these functions are appropriate for natural rivers and how they vary with factors  
794 including topography needs to be mapped out experimentally.  
795

796 It needs to be noted here that the precise formulation of the entrainment and deposition functions  
797 also affects steady state cover relations. When calibrating  $P$  on data, it cannot always be decided  
798 whether a specific deviation from the benchmark case results from varying entrainment and  
799 deposition processes or from changes in the probability function driven for example by variations in  
800 roughness. For the prediction of the steady state cover relations and for the comparison of data sets,  
801 this should not matter, but the dynamic evolution of cover could be strongly affected.  
802

803 The system timescale for cover adjustment is inversely related to transport capacity. This time scale  
804 can be long and in many realistic situations, cover cannot instantaneously adjust to changes in the  
805 forcing conditions. Thus, dynamic cover adjustment needs to be taken into account when modelling  
806 the long-term evolution of bedrock channels.  
807

808 Our model formulation implies that bedrock channels adjust bed cover to achieve grade. Therefore,  
809 bedrock channel evolution is driven by two optimization principles. On short time scales, bed cover  
810 adjusts to match the sediment output of a reach to its input. Over long time scales, width and slope  
811 of the channel evolve to match long-term incision rate to tectonic uplift or base level lowering rates.  
812

813 **Appendix A: Perturbation analysis**

814

815 Here, we derive the effect of a small sinusoidal perturbation of the driving variables, namely  
 816 sediment supply  $q_s^*$  and transport capacity  $q_t^*$ , on cover development. The perturbation of the  
 817 driving variables can be written as

818 
$$q_s^* = \bar{q}_s^* + \delta q_s^*$$

819 (eq. A1)

820 
$$q_t^* = \bar{q}_t^* + \delta q_t^*$$

821 (eq. A2)

822 Here, the bar denotes the average of the quantity at steady state, while  $\delta q_s^*$  and  $\delta q_t^*$  denote the  
 823 small perturbation. The exposed area can be similarly written as

824 
$$A^* = \bar{A}^* + \delta A^*$$

825 (eq. A3)

826 Steady state cover is directly related to the mass on the bed  $M_s^*$  by eq. (3), which we can rewrite as

827 
$$\frac{dA^*}{dt} = -P \frac{dM_s^*}{dt}$$

828 (eq. A4)

829 Substituting eq. (A3) and a similar equation for  $M_s^*$ ,

830 
$$M_s^* = \bar{M}_s^* + \delta M_s^*$$

831 (eq. A5)

832 we obtain

833 
$$\frac{d\delta A^*}{dt} = -P \frac{d\delta M_s^*}{dt}$$

834 (eq. A6)

835 Here, the averaged terms drop out as they are independent of time. If  $P$  and the steady state  
 836 solution for  $A^*$  are known, a direct relationship between  $A^*$  and  $M_s^*$  can be derived. For example, for  
 837 the exponential cover model (eq. 2), substituting eqs. (A3) and (A5), we find

838 
$$\bar{A}^* + \delta A^* = e^{-\bar{M}_s^* - \delta M_s^*} = e^{-\bar{M}_s^*} e^{-\delta M_s^*} = \bar{A}^* e^{-\delta M_s^*} \approx \bar{A}^* (1 - \delta M_s^*)$$

839 (eq. A7)

840 Here, since the  $\delta$  variables are small, we approximated the exponential term using a Taylor expansion  
 841 to first order. We obtain

842 
$$\delta A^* = -\bar{A}^* \delta M_s^*$$

843 (eq. A8)

844 It is therefore sufficient to derive the perturbation solution for  $M_s^*$ , the time evolution of which is  
 845 given by eq. (22). Eliminating  $M_m^*$  using eq. (24), we obtain

846 
$$\frac{\partial M_s^*}{\partial t^*} = \left(1 - e^{-q_s^*/U^*}\right) q_s^* - (1 - e^{-M_s^*}) q_t^*$$

847 (eq. A9)

848

849 **Perturbation of sediment supply**

850

851 First, let's look at a perturbation of sediment supply  $q_s^*$ , while other parameters are held constant.

852 Substituting eq. (A1) and (A5) into (A9), we obtain

853 
$$\frac{\partial \delta M_s^*}{\partial t^*} = \left(1 - e^{-(\bar{q}_s^* + \delta q_s^*)/U^*}\right) (\bar{q}_s^* + \delta q_s^*) - (1 - e^{-\bar{M}_s^* - \delta M_s^*}) q_t^*$$

854 (eq. A10)

855 Again, since the  $\delta$  variables are small, we can replace the relevant exponentials with Taylor expansion  
 856 to first order:

857 
$$e^{-\delta q_s^*/U^*} \approx 1 - \frac{\delta q_s^*}{U^*}$$

858 (eq. A11)

859 A similar approximation applies for the exponential in  $M_s^*$ . Substituting eq. (A11) into eq. (A10),  
860 expanding the multiplicative terms, dropping terms of second order in the  $\delta$  variables and  
861 rearranging, we get

862 
$$\frac{\partial \delta M_s^*}{\partial t^*} = \delta q_s^* \left( 1 - e^{-\bar{q}_s^*/U^*} + \frac{\bar{q}_s^*}{U^*} e^{-\bar{q}_s^*/U^*} \right) - \delta M_s^* \left( q_t^* - \left( 1 - e^{-\bar{q}_s^*/U^*} \right) \bar{q}_s^* \right)$$

863 (eq. A12)

864 The perturbation is assumed to be sinusoidal

865 
$$\delta q_s^* = d \sin\left(\frac{2\pi t}{p}\right)$$

866 (eq. A13)

867 Here,  $p$  is the period of the perturbation and  $d$  is its amplitude. Note that, to be consistent with the  
868 assumptions previously made,  $d$  needs to be small in comparison with the average sediment supply.  
869 Substituting, eq. (A12) can be integrated to obtain the solution

870 
$$\delta M_s^* = G_{q_s^*} \sin\left(\frac{2\pi t}{P} + \varphi_{q_s^*}\right) + C \exp\left\{ -\left( q_t^* - \left( 1 - e^{-\bar{q}_s^*/U^*} \right) \bar{q}_s^* \right) \frac{t}{T} \right\}$$

871 where  $C$  is a constant of integration. The gain is given by

872 
$$G_{q_s^*} = \frac{p}{T} \frac{\left( 1 - e^{-\bar{q}_s^*/U^*} + \frac{\bar{q}_s^*}{U^*} e^{-\bar{q}_s^*/U^*} \right) d}{\sqrt{\left( q_t^* - \left( 1 - e^{-\bar{q}_s^*/U^*} \right) \bar{q}_s^* \right)^2 \left( \frac{p}{T} \right)^2 + 4\pi^2}}$$

873 (eq. A14)

874 And the phase shift by

875 
$$\varphi_{q_s^*} = \tan^{-1} \left[ -\frac{2\pi}{\frac{p}{T} \left( q_t^* - \left( 1 - e^{-\bar{q}_s^*/U^*} \right) \bar{q}_s^* \right)} \right]$$

876 (eq. A15)

## 877 Perturbation of transport capacity

878

879 The perturbation of the transport capacity  $q_t^*$  is a little more complicated, since both  $q_t^*$  and  $U^*$  are  
880 explicitly dependent on hydraulics (e.g., shear stress; see eqs. 43 and 44), and thus  $U^*$  is implicitly  
881 dependent on  $q_t^*$  and  $\delta q_t^*$ . To circumvent this problem, we expand the exponential term featuring  
882  $U^*(\delta q_t^*)$  in eq. (A9) using a Taylor series expansion around  $\delta q_t^* = 0$ .

883

884 
$$\exp\left\{ -\frac{q_s^*}{U^*(\delta q_t^*)} \right\} \approx \exp\left\{ -\frac{q_s^*}{U^*(\delta q_t^* = 0)} \right\} \left[ 1 - \frac{q_s^*}{U^{*2}(\delta q_t^* = 0)} \frac{\partial U^*}{\partial \delta q_t^*} (\delta q_t^* = 0) \delta q_t^* \right]$$

885 (eq. A16)

886

887 Both  $U^*$  and its derivative are constants when evaluated at  $\delta q_t^* = 0$ . We can thus write

888

889 
$$\exp\left\{ -\frac{q_s^*}{U^*} \right\} = \exp\left\{ -\frac{q_s^*}{\bar{U}^*} \right\} \left[ 1 - \frac{q_s^*}{\bar{U}^{*2}} \overline{\left( \frac{\partial U^*}{\partial \delta q_t^*} \right)} \delta q_t^* \right] = [1 - C_0 \delta q_t^*] e^{-q_s^*/\bar{U}^*}$$

890

891 (eq. A17)

892 Here,  $C_0$  is a constant. Proceeding as before by substituting eq. (A2), (A8) and (A17) into (A9),  
 893 expanding exponential terms containing  $\delta$  variables, dropping terms of second order in the  $\delta$   
 894 variables and rearranging, we obtain:

$$895 \quad \frac{\partial \delta M_s^*}{\partial t^*} = \left( B q_s^* e^{-q_s^*/U^*} + e^{-M_s^*} - 1 \right) \delta q_t^* - \delta M_s^* \bar{q}_t^* e^{-M_s^*}$$

896 (eq. A18)

897 A sinusoidal perturbation of the form

$$898 \quad \delta q_t^* = d \sin\left(\frac{2\pi t}{p}\right)$$

899 (eq. A19)

900 yields the solution

$$901 \quad \delta M_s^* = G_{q_t^*} \sin\left(\frac{2\pi t}{p} + \varphi_{q_t^*}\right) + C \exp\left\{-\left(\bar{q}_t^* - \left(1 - e^{-q_s^*/U^*}\right) q_s^*\right) \frac{t}{p}\right\} \left\{-\left(\bar{q}_t^* - \left(1 - e^{-q_s^*/U^*}\right) q_s^*\right) \frac{t}{T}\right\}$$

902 with

$$903 \quad G_{q_t^*} = \frac{p}{T} \frac{\left(\frac{q_s^{*2}}{U^{*2}} \overline{\left(\frac{\partial U^*}{\partial \delta q_t^*}\right)} e^{-q_s^*/U^*} - \left(1 - e^{-q_s^*/U^*}\right) \frac{q_s^*}{\bar{q}_t^*}\right) d}{\sqrt{\bar{q}_t^{*2} \left(\frac{p}{T}\right)^2 \left(1 - \left(1 - e^{-q_s^*/U^*}\right) \frac{q_s^*}{\bar{q}_t^*}\right)^2 + 4\pi^2}}$$

904 (eq. A20)

905 and

$$906 \quad \varphi = \tan^{-1} \left( -\frac{2\pi}{\frac{p}{T} \left(\bar{q}_t^* - \left(1 - e^{-q_s^*/U^*}\right) q_s^*\right)} \right)$$

907 (eq. A21)

908

## 909 Summary

910

911 Using the system timescale  $T_s$ , the phase shift and gain can be generally rewritten as

912

$$913 \quad \varphi = \tan^{-1} \left( -2\pi \frac{T_s}{p} \right)$$

914 (eq. A22)

$$915 \quad G = \frac{p}{T_s} \frac{Kd}{\sqrt{\left(\frac{p}{T_s}\right)^2 + 4\pi^2}}$$

916 (eq. A23)

917 Here,  $K$  differs for perturbations in sediment supply and transport capacity, given by the equations

918

$$919 \quad K_{q_s^*} = 1 - e^{-\bar{q}_s^*/U^*} + \frac{\bar{q}_s^*}{U^*} e^{-\bar{q}_s^*/U^*}$$

920 (eq. A24)

$$921 \quad K_{q_t^*} = \frac{q_s^{*2}}{U^{*2}} \overline{\left(\frac{\partial U^*}{\partial \delta q_t^*}\right)} e^{-q_s^*/U^*} - \left(1 - e^{-q_s^*/U^*}\right) \frac{q_s^*}{\bar{q}_t^*}$$

922 (eq. A25)

923

924

|     |   |  |
|-----|---|--|
| 925 | <b>Notation</b>                           |  |
| 926 |   |  |
| 927 | Overbars denote time-averaged quantities. |  |
| 928 |   |  |
| 929 | $a$                                       | Shape parameter in the regularized incomplete Beta function.                             |
| 930 | $A^*$                                     | Fraction of exposed (uncovered) bed area.  |
| 931 | $A_c^*$                                   | Fraction of covered bed area.  |
| 932 | $b$                                       | Shape parameter in the regularized incomplete Beta function.                             |
| 933 | $B$                                       | Regularized incomplete Beta function.  |
| 934 | $C$                                       | Constant of integration.   |
| 935 | $C_0$                                     | Constant [ $\text{m}^2\text{s}/\text{kg}$ ].   |
| 936 | $d$                                       | Amplitude of perturbation [ $\text{kg}/\text{m}^2\text{s}$ ].                            |
| 937 | $D$                                       | Sediment deposition rate per bed area [ $\text{kg}/\text{m}^2\text{s}$ ].                |
| 938 | $D^*$                                     | Dimensionless sediment deposition rate.  |
| 939 | $D_{50}$                                  | Median grain size [m].   |
| 940 | $e$                                       | Base of the natural logarithm.   |
| 941 | $E$                                       | Sediment entrainment rate per bed area [ $\text{kg}/\text{m}^2\text{s}$ ].               |
| 942 | $E^*$                                     | Dimensionless sediment entrainment rate.   |
| 943 | $E_{max}$                                 | Maximal possible dimensionless sediment entrainment rate.                                |
| 944 | $g$                                       | Acceleration due to gravity [ $\text{m}/\text{s}^2$ ].                                   |
| 945 | $G$                                       | Gain [ $\text{kg}/\text{m}^2\text{s}$ ].   |
| 946 | $I$                                       | Non-dimensional incision rate.   |
| 947 | $k$                                       | Probability of sediment deposition on uncovered parts of the bed, linear implementation. |
| 948 |   |  |
| 949 | $k_I$                                     | Non-dimensional erodibility.   |
| 950 | $K$                                       | Parameter in the gain equation.  |
| 951 | $L$                                       | Characteristic length scale [m].   |
| 952 | $M_0$                                     | Minimum mass per area necessary to cover the bed [ $\text{kg}/\text{m}^2$ ].             |
| 953 | $M_0^*$                                   | Dimensionless characteristic sediment mass.  |
| 954 | $M_m$                                     | Mobile sediment mass [ $\text{kg}/\text{m}^2$ ].   |
| 955 | $M_m^*$                                   | Dimensionless mobile sediment mass.  |
| 956 | $M_s$                                     | Stationary sediment mass [ $\text{kg}/\text{m}^2$ ].                                     |
| 957 | $M_s^*$                                   | Dimensionless stationary sediment mass.  |
| 958 | $p$                                       | Period of perturbation [s].  |
| 959 | $p_c$                                     | Probability of entrainment, CA model, blocked grains.                                    |
| 960 | $p_i$                                     | Probability of entrainment, CA model, free grains.                                       |
| 961 | $P$                                       | Probability of sediment deposition on uncovered parts of the bed.                        |
| 962 | $q_s$                                     | Mass sediment transport rate per unit width [ $\text{kg}/\text{ms}$ ].                   |
| 963 | $q_s^*$                                   | Dimensionless sediment transport rate.   |
| 964 | $q_t$                                     | Mass sediment transport capacity per unit width [ $\text{kg}/\text{ms}$ ].               |
| 965 | $q_t^*$                                   | Dimensionless transport capacity.  |
| 966 | $Q_s^*$                                   | Relative sediment supply; sediment transport rate over transport capacity.               |
| 967 | $Q_t$                                     | Mass sediment transport capacity [ $\text{kg}/\text{s}$ ].                               |
| 968 | $t$                                       | Time variable [s].   |
| 969 | $t^*$                                     | Dimensionless time.  |
| 970 | $T$                                       | Characteristic time scale [s].   |
| 971 | $T_E$                                     | Characteristic time scale for sediment entrainment [s].                                  |
| 972 | $T_S$                                     | Characteristic system time scale [s].  |

|     |            |   |
|-----|------------|---|
| 973 | $U$        | Sediment speed [m/s].   |
| 974 | $U^*$      | Dimensionless sediment speed.   |
| 975 | $x$        | Dimensional streamwise spatial coordinate [m].                                |
| 976 | $x^*$      | Dimensionless streamwise spatial coordinate.                                  |
| 977 | $y$        | Dummy variable.   |
| 978 | $\alpha$   | Exponent.   |
| 979 | $\gamma$   | Fraction of pore space in the sediment.                                       |
| 980 | $\delta$   | denotes time-varying component.   |
| 981 | $\theta$   | Shields stress.   |
| 982 | $\theta_c$ | Critical Shields stress.  |
| 983 | $\rho$     | Density of water [kg/m <sup>3</sup> ].  |
| 984 | $\rho_s$   | Density of sediment [kg/m <sup>3</sup> ].                                     |
| 985 | $\tau$     | Bed shear stress [N/m <sup>2</sup> ].   |
| 986 | $\tau_c$   | Critical bed shear stress at the onset of bedload motion [N/m <sup>2</sup> ]. |
| 987 |            |   |
| 988 |            |   |

989 **Acknowledgements**

990

991 We thank Joel Scheingross and Jean Braun for insightful discussions and two anonymous reviewers  
992 from insightful comments on a previous version of the manuscript. The data from the Erlenbach is  
993 owned by and is used with permission of the Mountain Hydrology and Mass Movements Group at  
994 the Swiss Federal Research Institute for Forest Snow and Landscape Research WSL.

995

996 **References**

997

998 Aubert, G., Langlois, V.J., Allemand, P. (2016). Bedrock incision by bedload: Insights from direct  
999 numerical simulations. *Earth Surf. Dynam.*, 4, 327-342, doi: 10.5194/esurf-4-327-2016

1000 Beer, A. R., & Turowski, J. M. (2015). Bedload transport controls bedrock erosion under sediment-  
1001 starved conditions. *Earth Surface Dynamics*, 3, 291-309, doi: 10.5194/esurf-3-291-2015

1002 Beer, A. R., Turowski, J. M., Fritschi, B., Rieke-Zapp, D. H. (2015). Field instrumentation for high-  
1003 resolution parallel monitoring of bedrock erosion and bedload transport, *Earth Surface  
1004 Processes and Landforms*, 40, 530-541, doi: 10.1002/esp.3652

1005 Beer, A. R., Kirchner, J. W., Turowski, J. M. (2016). Graffiti for science – erosion painting reveals  
1006 spatially variable erosivity of sediment-laden flows, *Earth Surface Dynamics*, 4, 885-894, doi:  
1007 10.5194/esurf-4-885-2016

1008 Charru, F., Mouilleron, H., Eiff, O. (2004). Erosion and deposition of particles on a bed sheared by a  
1009 viscous flow. *J. Fluid Mech.*, 519, 55-80

1010 Chatanantavet, P. & Parker, G. (2008). Experimental study of bedrock channel alluviation under  
1011 varied sediment supply and hydraulic conditions. *Water Resour. Res.*, 44, W12446, doi:  
1012 10.1029/2007WR006581

1013 Cook, K.; Turowski, J. M. & Hovius, N. (2013). A demonstration of the importance of bedload  
1014 transport for fluvial bedrock erosion and knickpoint propagation. *Earth Surf. Process.  
1015 Landforms*, 38, 683-695, doi: 10.1002/esp.3313

1016 Fernandez Luque, R. & van Beek, R. (1976). Erosion and transport of bed-load sediment. *J. Hydraul.  
1017 Res.*, 14, 127-144

1018 Finnegan, N. J.; Sklar, L. S. & Fuller, T. K. (2007). Interplay of sediment supply, river incision, and  
1019 channel morphology revealed by the transient evolution of an experimental bedrock channel.  
1020 *Journal of Geophysical Research*, 112, F03S11, doi: 10.1029/2006JF000569

1021 Gilbert, G. K. (1877), Report on the geology of the Henry Mountains: Geographical and geological  
1022 survey of the Rocky Mountain region, U.S. Gov. Print. Off., Washington, D. C.

1023 Hobley, D. E. J.; Sinclair, H. D.; Mudd, S. M. & Cowie, P. A. (2011). Field calibration of sediment flux  
1024 dependent river incision. *J. Geophys. Res.*, 116, F04017, doi: 10.1029/2010JF001935

1025 Hodge, R.A. (in press) Sediment processes in bedrock-alluvial rivers: Research since 2010 and  
1026 modelling the impact of fluctuating sediment supply on sediment cover. In: Tsutsumi, D. &  
1027 Laronne, J. *Gravel-Bed Rivers: Process and Disasters*. Wiley-Blackwell.

1028 Hodge, R. A. & Hoey, T. B. (2012). Upscaling from grain-scale processes to alluviation in bedrock  
1029 channels using a cellular automaton model. *J. Geophys. Res.*, 117, F01017, doi:  
1030 10.1029/2011JF002145

1031 Hodge, R. A., T. B. Hoey, and L. S. Sklar (2011), Bedload transport in bedrock rivers: the role of  
1032 sediment cover in grain entrainment, translation and deposition, *J. Geophys. Res.*, 116,  
1033 F04028, doi: 10.1029/2011JF002032.

1034 Hodge, R. A., and T. B. Hoey (2016), A Froude scale model of a bedrock-alluvial channel reach: 2.  
1035 Sediment cover, *J. Geophys. Res.*, in press, doi: 10.1002/2015JF003709

1036 Inoue, T., N. Izumi, Y. Shimizu, G. Parker (2014). Interaction among alluvial cover, bed roughness, and  
1037 incision rate in purely bedrock and alluvial-bedrock channel. *J. Geophys. Res.*, 119, 2123-  
1038 2146, doi: 10.1002/2014JF003133

1039 Inoue, T., T. Iwasaki, G. Parker, Y. Shimizu, N. Izumi, C.P. Stark, J. Funaki (2016). Numerical simulation  
1040 of effects of sediment supply on bedrock channel morphology. *J. Hydr. Eng.*, in press, doi:  
1041 10.1061/(ASCE)HY.1943-7900.0001124

1042 Johnson, J.P.L. (2014). A surface roughness model for predicting alluvial cover and bed load transport  
1043 rate in bedrock channels. *J. Geophys. Res.*, 119, 2147-2173, doi: 10.1002/2013JF003000

1044 Johnson, J. P. & Whipple, K. X. (2007). Feedbacks between erosion and sediment transport in  
1045 experimental bedrock channels. *Earth Surf. Process. Landforms*, 32, 1048-1062, doi:  
1046 10.1002/esp.1471

1047 Lague, D. (2010). Reduction of long-term bedrock incision efficiency by short-term alluvial cover  
1048 intermittency. *J. Geophys. Res.*, 115, F02011, doi:10.1029/2008JF001210

1049 Lajeunesse, E.; Malverti, L. & Charru, F. (2010). Bed load transport in turbulent flow at the grain  
1050 scale: Experiments and modeling. *Journal of Geophysical Research*, 115, F04001

1051 Paola, C. & Voller, V. R. (2005). A generalized Exner equation for sediment mass balance. *J. Geophys.*  
1052 *Res.*, 110, F04014

1053 Phillips, C.B., D.J. Jerolmack (2016). Self-organization of river channels as a critical filter on climate  
1054 signals. *Science*, 352, 694-697

1055 Mackin JH. (1948). Concept of the graded river. *Geological Society of America Bulletin* **59**: 463-512.  
1056 doi: 10.1130/0016-7606(1948)59[463:COTGR]2.0.CO;2

1057 Meyer-Peter, E., and R. Mueller (1948). Formulas for bedload transport, in 2nd meeting Int. Assoc.  
1058 Hydraulic Structures Res., edited, Stockholm, Sweden.

1059 Molnar P, Densmore AL, McArdell BW, Turowski JM, Burlando P. (2010). Analysis of changes in the  
1060 step-pool morphology and channel profile of a steep mountain stream following a large  
1061 flood. *Geomorphology* 124: 85–94. DOI. 10.1016/j.geomorph.2010.08.014

1062 Nelson, P. A., and G. Seminara (2011), Modeling the evolution of bedrock channel shape with erosion  
1063 from saltating bed load, *Geophys. Res. Lett.*, 38, L17406, doi: 10.1029/2011GL048628

1064 Nelson, P. A., and G. Seminara (2012), A theoretical framework for the morphodynamics of bedrock  
1065 channels, *Geophys. Res. Lett.*, 39, L06408, doi: 10.1029/2011GL050806.

1066 Nitsche, M., D. Rickenmann, J.M. Turowski, A. Badoux, J.W. Kirchner, (2011). Evaluation of bedload  
1067 transport predictions using flow resistance equations to account for macro-roughness in  
1068 steep mountain streams, *Water Resources Research*, 47, W08513, doi:  
1069 10.1029/2011WR010645

1070 Rickenmann D, Turowski JM, Fritschi B, Klaiber A, Ludwig A. (2012). Improved sediment transport  
1071 measurements in the Erlenbach stream including a moving basket system. *Earth Surface*  
1072 *Processes and Landforms* 37: 1000–1011, doi: 10.1002/esp.3225

1073 Sklar, L. S. & Dietrich, W. (1998). River longitudinal profiles and bedrock incision models: Stream  
1074 power and the influence of sediment supply. In: *Rivers over Rock: Fluvial Processes in*  
1075 *Bedrock Channels*, E. Tinkler, K. J. & Wohl, E. E. (Eds.), American Geophysical Union, 107, 237-  
1076 260

1077 Sklar, L.S., Dietrich, W.E., (2001). Sediment and rock strength controls on river incision into bedrock.  
1078 *Geology* 29, 1087-1090, doi: 10.1130/0091-7613(2001)029<1087:SARSCO>2.0.CO;2

1079 Sklar, L. S. & Dietrich, W. E. (2004). A mechanistic model for river incision into bedrock by saltating  
1080 bed load. *Water Resour. Res.*, 40, W06301, doi: 10.1029/2003WR002496

1081 Turowski, J. M. (2009). Stochastic modeling of the cover effect and bedrock erosion. *Water Resour.*  
1082 *Res.*, 45, W03422, doi: 10.1029/2008WR007262

1083 Turowski, J. M. & Bloem, J.-P. (2016). The influence of sediment thickness on energy delivery to the  
1084 bed by bedload impacts. *Geodinamica Acta*, 28, 199-208, doi:  
1085 10.1080/09853111.2015.1047195

1086 Turowski, J. M. & Rickenmann, D. (2009). Tools and cover effects in bedload transport observations  
1087 in the Pitzbach, Austria. *Earth Surf. Process. Landforms*, 34, 26-37, doi: 10.1002/esp.1686

1088 Turowski, J. M.; Lague, D. & Hovius, N. (2007). Cover effect in bedrock abrasion: A new derivation  
1089 and its implication for the modeling of bedrock channel morphology. *J. Geophys. Res.*, 112,  
1090 F04006, doi: 10.1029/2006JF000697

1091 Turowski, J. M.; Hovius, N.; Hsieh, M.-L.; Lague, D. & Chen, M.-C. (2008). Distribution of erosion  
1092 across bedrock channels. *Earth Surf. Process. Landforms*, 33, 353-363, doi: 10.1002/esp.1559

1093 Turowski JM, Yager EM, Badoux A, Rickenmann D, Molnar P. (2009). The impact of exceptional  
1094 events on erosion, bedload transport and channel stability in a step-pool channel. *Earth*  
1095 *Surface Processes and Landforms* 34: 1661–1673, doi: 10.1002/esp.1855

1096 Turowski, J.M., A. Badoux, J. Leuzinger, R. Hegglin (2013). Large floods, alluvial overprint, and  
1097 bedrock erosion. *Earth Surface Processes and Landforms*, 38, 947-958, doi: 10.1002/esp.3341

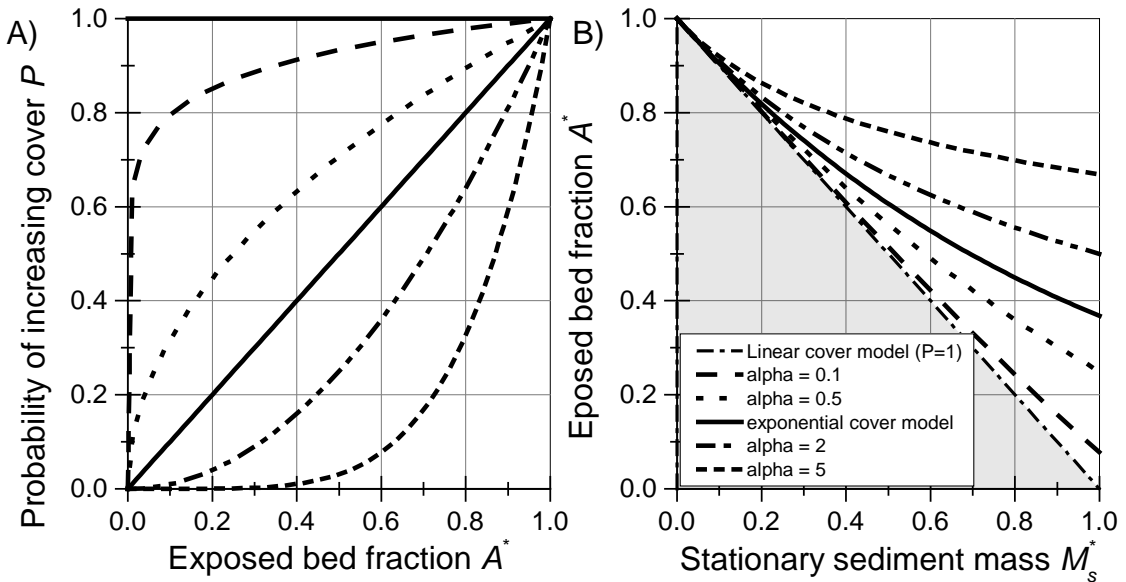
1098 Wohl, E. E. & Ikeda, H. (1997). Experimental simulation of channel incision into a cohesive substrate  
1099 at varying gradients. *Geology*, 25, 295-298, doi: 10.1130/0091-  
1100 7613(1997)025<0295:ESOCII>2.3.CO;2

1101 Wyss, C.R., D. Rickenmann, B. Fritschi, J.M. Turowski, V. Weitbrecht, R.M. Boes, (2016). Measuring  
1102 bedload transport rates by grain-size fraction using the Swiss Plate Geophone signal at the  
1103 Erlenbach, *Journal of Hydraulic Engineering*, 142(5), 04016003, doi: 10.1061/(ASCE)HY.1943-  
1104 7900.0001090

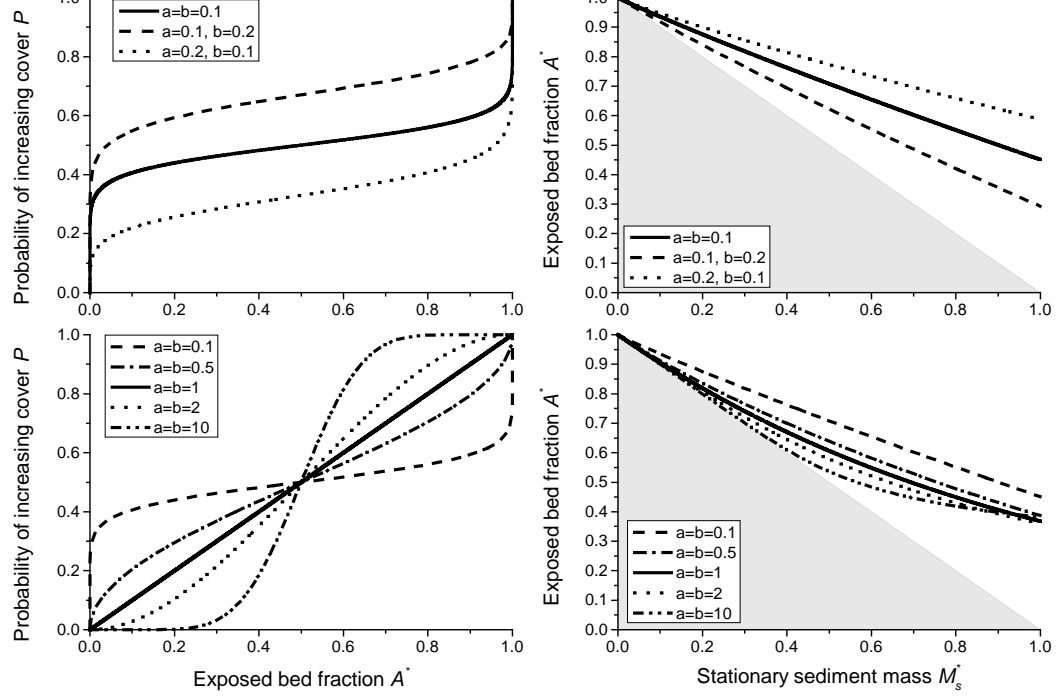
1105 Yanites, B. J.; Tucker, G. E.; Hsu, H.-L.; Chen, C.-C.; Chen, Y.-G. & Mueller, K. J. (2011). The influence of  
1106 sediment cover variability on long-term river incision rates: An example from the Peikang  
1107 River, central Taiwan. *J. Geophys. Res.*, 116, F03016, doi: 10.1029/2010JF001933

1108 Zhang, L., G. Parker, C.P. Stark, T. Inoue, E. Viparelli, X. Fu, N. Izumi (2015). Macro-roughness model  
1109 of bedrock-alluvial river morphodynamics. *Earth Surface Dynamics*, 3, 113-138, doi:  
1110 10.5194/esurf-3-113-2015

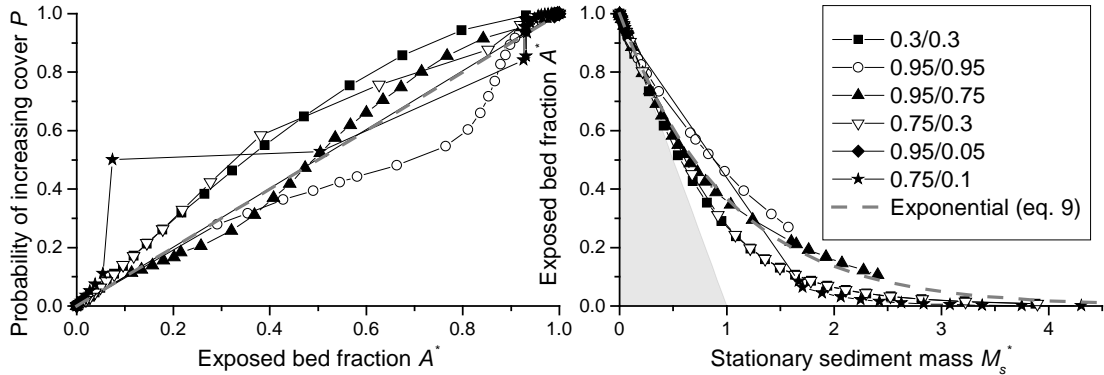
1111



1112  
1113 Fig. 1: A) Various examples for the probability function  $P$  as a function of bedrock exposure  $A^*$ . B)  
1114 Corresponding analytical solutions for the cover function between  $A^*$  and dimensionless sediment  
1115 mass  $M_s^*$  using eq. (7), (9) and (10). Grey shading depicts the area where the cover function cannot  
1116 run due to conservation of mass.

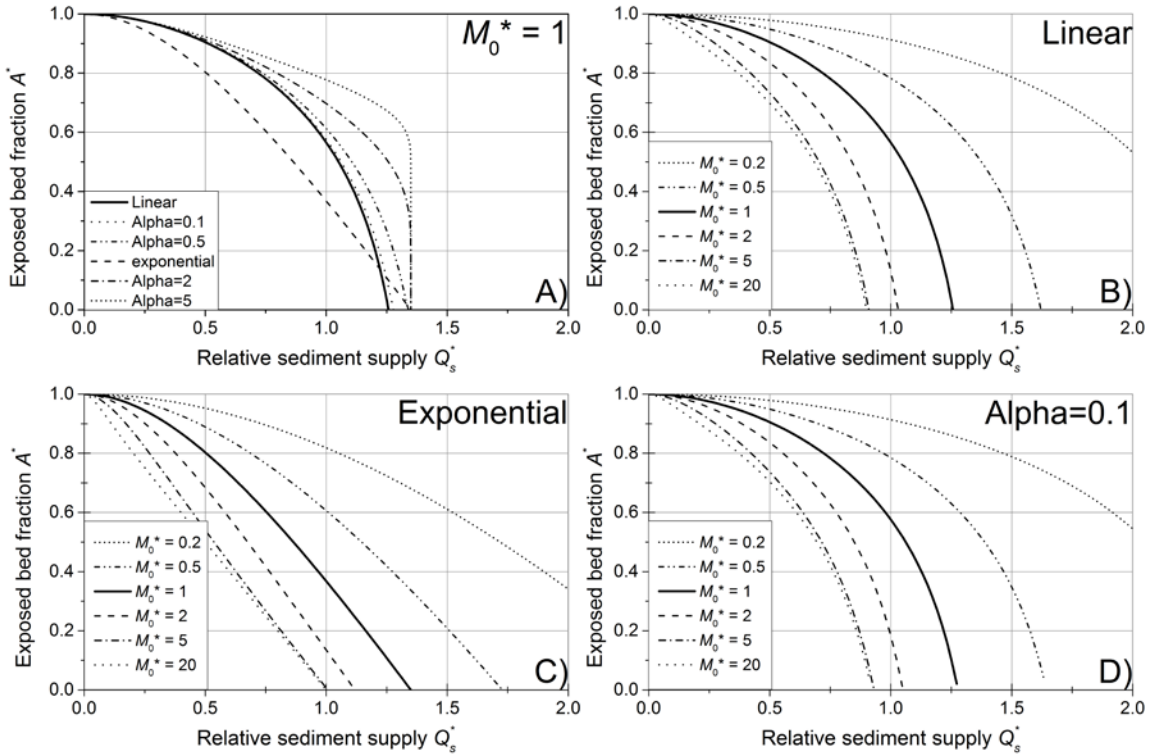


1118  
1119 Fig. 2: Examples for the use of the regularized incomplete Beta function (eq. 12) to parameterize  $P$ ,  
1120 using various values for the shape parameters  $a$  and  $b$ . The choice  $a = b = 1$  gives a dependence that  
1121 is equivalent to the exponential cover function. Grey shading depicts the area where the cover  
1122 function cannot run due to conservation of mass.



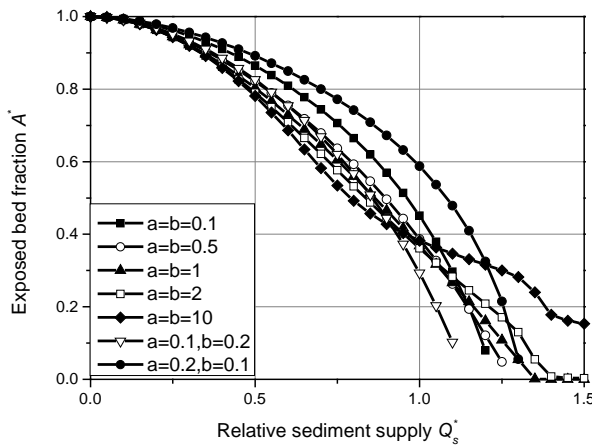
1123  
1124  
1125  
1126  
1127  
1128

Fig. 3: Probability functions  $P$  and cover function derived from data obtained from the model of Hodge and Hoey (2012). The grey dashed line shows the exponential benchmark behavior. Grey shading depicts the area where the cover function cannot run due to conservation of mass. The legend gives values of  $P_i$  and  $P_c$  used for the runs (see text).

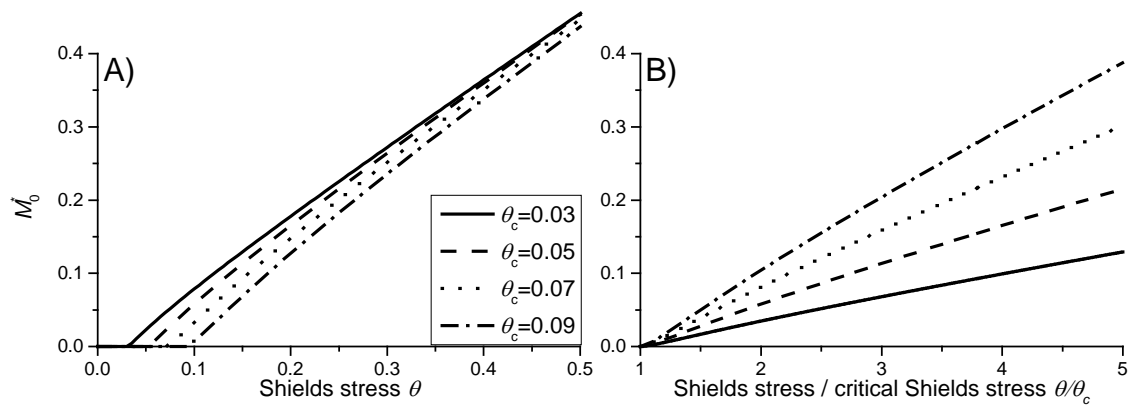


1129  
1130  
1131  
1132  
1133  
1134

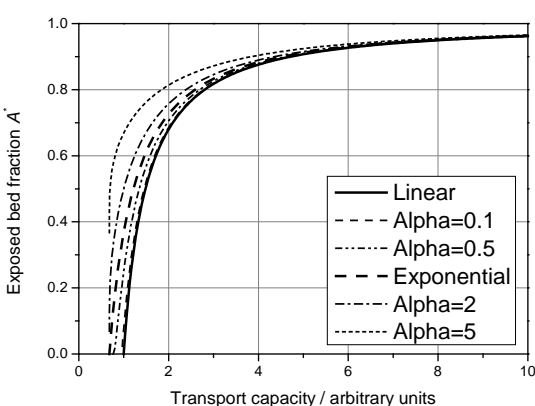
Fig. 4: Analytical solutions at steady state for the exposed fraction of the bed ( $A^*$ ) as a function of relative sediment supply ( $Q^*$ , cf. Fig. 1). A) Comparison of the different solutions, keeping  $M_0^*$  constant at 1. B) Varying  $M_0^*$  for the linear case (eq. 31). C) Varying  $M_0^*$  for the exponential case (eq. 30). D) Varying  $M_0^*$  for the power law case with  $\alpha = 0.1$  (eq. 32).



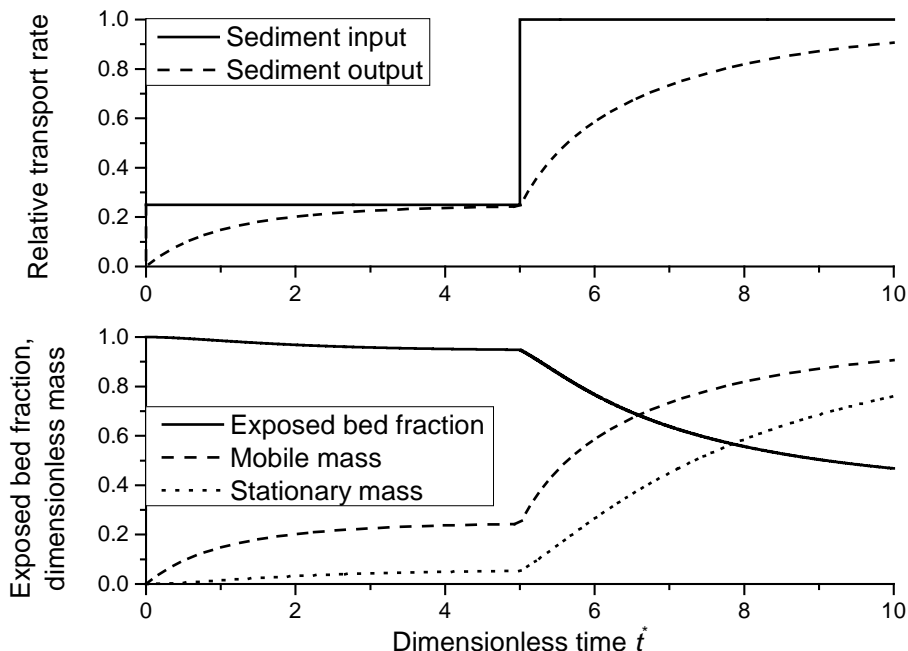
1135  
1136 Fig. 5: Steady state solutions using the beta distribution to parameterize  $P$  (eq. 11) for a range of  
1137 parameters  $a$  and  $b$ , and using  $M_0^* = 1$  (cf. Fig. 2). The solutions were obtained by iterating the  
1138 equations to a steady state, using initial conditions of  $A^* = 1$  and  $M_m^* = M_s^* = 0$ .  
1139



1140  
1141 Fig. 6: The characteristic dimensionless mass  $M_0^*$  depicted as a function of A) the Shields stress and  
1142 B) the ratio of Shields stress to critical Shields stress (eq. 37).  
1143

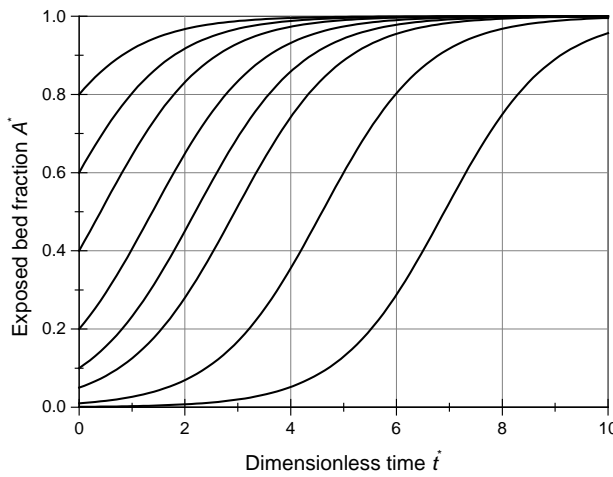


1144  
1145 Fig. 7: Variation of the exposed bed fraction as a function of transport capacity, assuming that  
1146 particle speed scales with transport capacity to the power of one third.  
1147  
1148



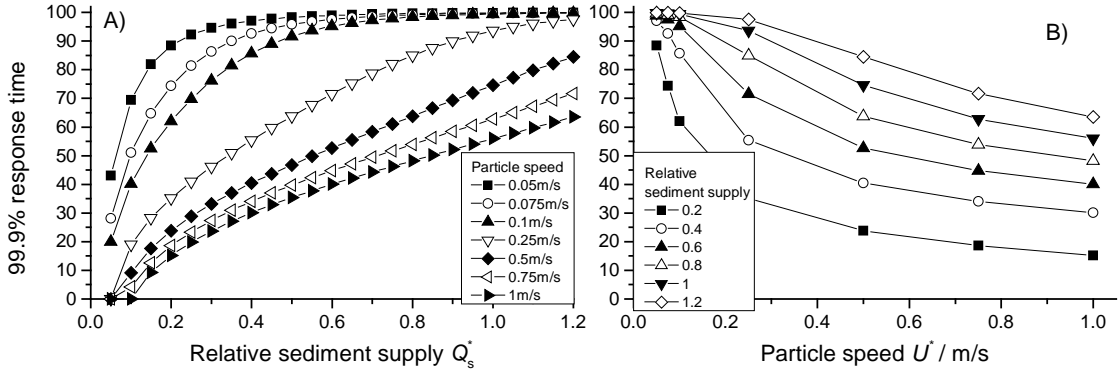
1149  
1150  
1151  
1152  
1153  
1154

Fig. 8: Temporal evolution of cover for the simple case of a control box with sediment through-flux, based on eqs. (3), (22), (23) and (24). Relative sediment supply (supply normalized by transport capacity) was specified to 0.25 and increased to 1 at  $t^* = 5$ . The response of sediment output, mobile and stationary sediment mass and the exposed bed fraction was calculated. Here, we used the exponential function for  $P$  (eq. 9) and  $M_0^* = U^* = 1$ . The initial values were  $A^* = 1$  and  $M_m^* = M_s^* = 0$ .

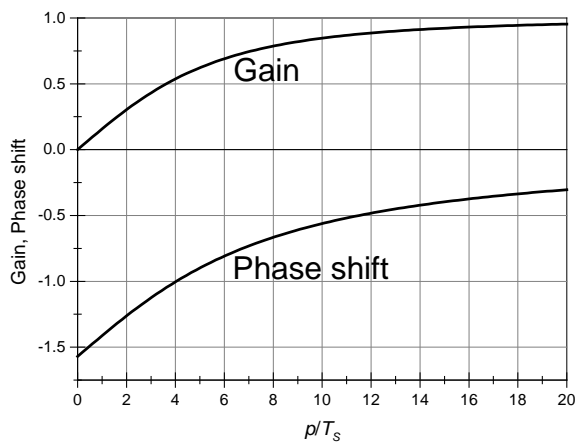


1155  
1156  
1157  
1158  
1159

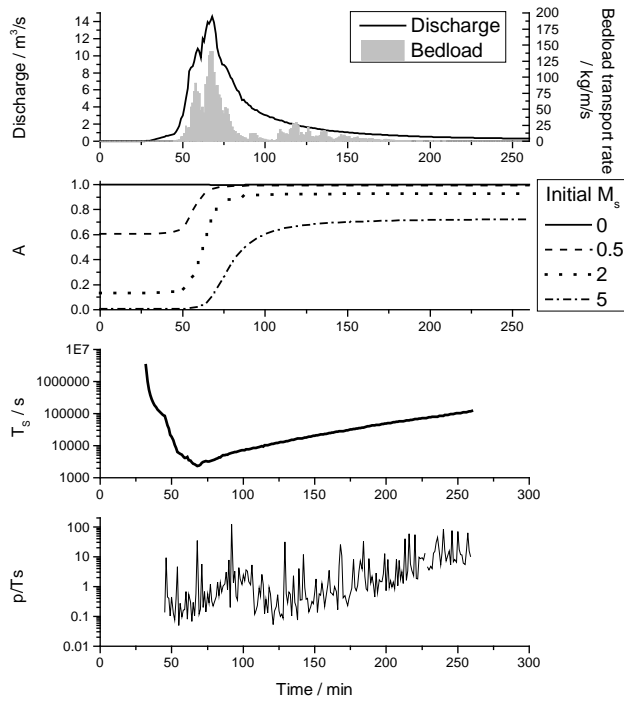
Fig. 9: Evolution of the exposed bed fraction (removal of sediment cover) over time starting with different initial values of bed exposure, for the special case of no sediment supply, i.e.,  $q_s^* = 0$  (eq. 41) and  $q_t^* = 1$ .



1160  
1161 Fig. 10: Dimensionless time to reach 99.9% of the total adjustment in exposed area as a function of  
1162 A) transport stage and B) particle speed. All simulation were started with  $A^* = 1$  and  $M_m^* = M_s^* = 0$ .  
1163



1164  
1165 Fig. 11: Phase shift (eq. 50) and gain (eq. 51) as a function of the ratio of the period of perturbation  $p$   
1166 and the system time scale  $T_s$ . For the calculation, the constant factor in the gain ( $Kd$ ) was set equal to  
1167 one.  
1168



1169  
 1170 Fig. 12: Calculated evolution of cover during the largest event observed at the Erlenbach on 20<sup>th</sup> June  
 1171 2007 (Turowski et al., 2009). Bedload transport rates were measured with the Swiss Plate geophone  
 1172 sensors calibrated with direct bedload samples (Rickenmann et al., 2012). The final fraction of  
 1173 exposed bedrock is strongly dependent on its initial value.  
 1174